Inhomogeneous Random Phase Approximation: A Solvable Model

J.C. Lemm
Institut für Theoretische Physik I, Universität Münster,
48149 Münster, Germany

February 8, 1995

Abstract

A recently developed method to include particle–hole correlations into the time–independent mean field theory for scattering (TIMF) by an inhomogeneous random phase approximation (IRPA) is applied to a numerically solvable model. Having adapted the procedure according to numerical requirements, IRPA calculations turn out to be tractable. The obtained results improve TIMF results.

Proposed running head: IRPA: A Solvable Model

Dr. Jörg C. Lemm
Institut für Theoretische Physik I
Wilhelm–Klemm–Str. 9
D-48149 Münster
Germany

Phone : (011) 49 251 83 4922
Fax : (011) 49 251 83 4962
Email : lemm@lorentz.uni-muenster.de

Contents

1 Introduction **5**

2 The Model **5**

3 The Exact Solution **7**

4 The TIMF Aproximation **8**

5 Inhomogeneous RPA (IRPA) **14**

6 IRPA with Square Integrable Particle Orbitals (SIRPA) **19**

7 Numerical Results **23**

8 Summarizing the Results for the Solvable Model **31**

9 Conclusion **32**

1 Introduction

This is the second of two papers the first [1] of which contains the theoretical framework while the present one concentrates on numerical application. In [1, 2] a second quantized formulation of TIMF has been developed for calculating matrix elements of the resolvent $\mathcal{G} = (E - \mathcal{H})^{-1}$, as well as of the nontrivial part of the transition operator $\Delta T = \mathcal{V}'\mathcal{G}\mathcal{V}$, where $\mathcal{V}'$ and $\mathcal{V}$ stand for the prior and post potentials defined by the in and out channels, respectively. Rewriting the inhomogeneous variational equations, which are the basis of TIMF, as a diagonalization problem, allows to introduce particle–hole correlations in terms of a generalized nonhermitian RPA technique. In this paper the new method is studied with the help of a model, where in addition to a TIMF and IRPA solution, an exact solution is possible as well. The issue of this paper is to explore the actual tractability of the generalized RPA method and to verify the quality of the IRPA results by comparing them with the TIMF approximation and the exact solution.

2 The Model

As a simple case of an operator inversion we consider the calculation of diagonal elements $<\chi\,|\,\mathcal{G}(E)\,|\,\chi>$ of the resolvent $\mathcal{G}(E) = 1/(E - \mathcal{H})$ of a Hamiltonian $\mathcal{H}$. Firstly, we want to study some technical questions and possibilities of the IRPA method. Secondly, we are interested in testing the quality of such an approximation. We need therefore a solvable model for which we can perform, besides TIMF and IRPA calculations, an exact calculation which enables us to see whether the TIMF solution is improved by an IRPA. Hence we consider a one–dimensional two–particle model for which we can easily find an exact solution. In particular, we choose as test problem a one–dimensional, two–particle model with a correct treatment of the center–of–mass term and a Galilei–invariant, separable potential with a Gaussian shape in the momentum space. From the total Hamiltonian we subtract the center–of–mass part $\mathcal{H}_{c.m.} = \frac{Q^2}{4}$, with $Q = q_1 + q_2$, which allows to separate the irrelevant center–of–mass motion. The Hamiltonian of relative motion $\mathcal{H}$ for the model is defined by its matrix elements in momentum space, with q_1, q_2 denoting the single–particle momenta for the two particles, [3]

$$<q_1'q_2'\,|\,\mathcal{H}\,|\,q_1q_2>=<q_1'q_2'\,|\,(\mathcal{T}+\mathcal{V}-\mathcal{H}_{c.m.})\,|\,q_1q_2>= \qquad (1)$$

$$\left[\frac{q_1^2}{2}+\frac{q_2^2}{2}-\frac{(q_1+q_2)^2}{4}\right]\delta(q_1-q_1')\delta(q_2-q_2')-\delta(q_1+q_2-q_1'-q_2')$$
$$\times\frac{1}{4}\lambda\nu^2(q_1-q_2)\exp[-\frac{1}{4}\nu^2(q_1-q_2)^2](q_1'-q_2')\exp[-\frac{1}{4}\nu^2(q_1'-q_2')^2],$$

having set $\hbar^2/m=1$. In the following we choose $\nu=1$. The subtraction of $\mathcal{H}_{c.m.}$ gives rise to the two–body operator $-q_1q_2/2$ which is analogous to an additional two–body potential.

While TIMF as a mean field approximation is formulated in single–particle coordinates, an exact solution is most easily found using the center–of–mass and relative momenta $Q=q_1+q_2$ and $q=(q_1-q_2)/2$. In this picture the matrix elements of the Hamiltonian are written as

$$\begin{aligned}&<q'Q'\,|\,\mathcal{H}\,|\,qQ>= \\ &\quad\delta(Q-Q')\left[q^2\delta(q-q')-\lambda\nu^2 qq'\exp(-\nu^2q^2)\exp(-\nu'^2q'^2)\right].\end{aligned}\tag{2}$$

The factor $\delta(Q-Q')$ shows that the center–of–mass motion is not influenced by the potential. According to (2) the potential $\mathcal{V}$ has the separable form

$$\mathcal{V}=-\lambda\delta(Q-Q')|\,\nu><\nu\,|,\tag{3}$$

with the form factor

$$<q\,|\,\nu>=\nu q\exp\left[-\nu^2q^2\right].\tag{4}$$

As wave packets for the channel wave functions, antisymmetrized Gaussians boosted by $\pm k=\pm\sqrt{\mathrm{Re}(E)}$ are appropriate. With

$$\chi_{(+k)}(q_1) = \pi^{-1/4}b^{1/2}\exp\left\{-\frac{1}{2}b^2[(q_1-k)^2]\right\},\tag{5}$$
$$\chi_{(-k)}(q_2) = \pi^{-1/4}b^{1/2}\exp\left\{-\frac{1}{2}b^2[(q_2+k)^2]\right\},\tag{6}$$

the antisymmetrized channel wave function reads

$$\chi(q_1,q_2,k)=\chi'(q_1,q_2,k)=\frac{1}{\sqrt{2}}\left[\chi_{(+k)}(q_1)\chi_{(-k)}(q_2)-\chi_{(-k)}(q_1)\chi_{(+k)}(q_2)\right]$$
$$=\frac{1}{\sqrt{2}}\pi^{-1/2}b\left[\exp\left\{-\frac{1}{2}b^2[(q_1-k)^2+(q_2+k)^2]\right\}\right.$$

$$- \exp\left\{-\frac{1}{2}b^2[(q_1+k)^2+(q_2-k)^2]\right\}\Bigg]. \tag{7}$$

The width b is chosen equal to 1 in the following. Written in center–of–mass and relative coordinates we have

$$\chi(q,Q,k) = \chi_r(q,k)\chi_{c.m.}(Q,k) = \left[\pi^{-1/4}\left[\frac{b}{\sqrt{2}}\right]^{1/2}\exp(-\frac{1}{4}b^2Q^2)\right]$$

$$\times\left[\frac{1}{\sqrt{2}}\pi^{-1/4}(b\sqrt{2})^{1/2}\left\{\exp[-b^2(q-k)^2]-\exp[-b^2(q+k)^2]\right\}\right], \tag{8}$$

using r and $c.m.$ as index for the relative or center–of–mass motion, respectively.

3 The Exact Solution

The exact diagonal amplitude for $\chi' = \chi$ is given as

$$D = <\chi\,|\,\mathcal{G}(E)\,|\,\chi> = <\chi\,|\Psi>, \tag{9}$$

with Ψ defined by

$$(E-\mathcal{H})|\,\Psi> = |\,\chi>. \tag{10}$$

Because $\mathcal{H}$ leaves the center–of–mass motion invariant, we are only interested in the relative motion part of $\Psi = \Psi_r\chi_{c.m.}$. Thus (10) becomes

$$(E-\mathcal{H})|\Psi_r> \;=\; |\chi_r> \tag{11}$$

or alternatively

$$\begin{aligned}(E-\mathcal{H}_0)|\Psi_r> &= |\,\chi_r> + \mathcal{V}|\,\Psi_r> \\ &= |\,\chi_r> - \lambda|\,\nu><\nu\,|\,\Psi_r>,\end{aligned} \tag{12}$$

using (3) for the potential and $\mathcal{H}_0 = \mathcal{H} - \mathcal{V}$. Inversion yields

$$|\,\Psi_r> = \mathcal{G}_0|\,\chi_r> - \lambda\mathcal{G}_0|\,\nu><\nu\,|\,\Psi_r>, \tag{13}$$

with $\mathcal{G}_0 = (E-\mathcal{H}_0)^{-1}$. Projecting onto $<\nu\,|$ leads to

$$<\nu\,|\,\Psi_r> = \frac{<\nu\,|\,\mathcal{G}_0\,|\,\chi_r>}{1+\lambda<\nu\,|\,\mathcal{G}_0\,|\,\nu>}, \tag{14}$$

or, substituting into (13),

$$|\,\Psi_r\!> = \mathcal{G}_0|\,\chi_r\!> - \lambda\mathcal{G}_0|\,\nu\!>\frac{<\nu\,|\,\mathcal{G}_0\,|\,\chi_r\!>}{1+\lambda<\nu\,|\,\mathcal{G}_0\,|\,\nu\!>}. \tag{15}$$

This gives as exact amplitude according to Eq.(9)

$$\begin{aligned} D &= \;<\chi_r\,|\,\mathcal{G}_0\,|\,\chi_r\!> -\lambda\frac{<\chi_r\,|\,\mathcal{G}_0\,|\,\nu\!><\nu\,|\,\mathcal{G}_0\,|\,\chi_r\!>}{1+\lambda<\nu\,|\,\mathcal{G}_0\,|\,\nu\!>} \\ &= \;<\chi_r\,|\,\mathcal{G}_0\,|\,\chi_r\!> -\lambda\frac{<\nu\,|\,\mathcal{G}_0\,|\,\chi_r\!>^2}{1+\lambda<\nu\,|\,\mathcal{G}_0\,|\,\nu\!>}, \end{aligned} \tag{16}$$

since $<q\,|\,\nu>$ as well as $<q\,|\,\chi_r>$ are real. The occurring integrals can be solved numerically without problems.

4 The TIMF Aproximation

For TIMF we use trial functions restricted to Slater determinants, and calculate the single–particle variational equations of a suitable functional which has the exact diagonal amplitude D as stationary value for unrestricted variations of the trial functions. Let us consider the additive TIMF functional [1]

$$F(\Phi,\Phi') = <\Phi'\,|\,\chi\!> + <\chi'\,|\,\Phi\!> - <\Phi'\,|\,(E-\mathcal{H})\,|\,\Phi\!>. \tag{17}$$

If the normalization factors of Φ, Φ' are taken into account correctly, this implies in the case of stationarity the relations

$$<\Phi'\,|\,\chi\!> = <\chi'\,|\,\Phi\!> = <\Phi'\,|\,(E-\mathcal{H})\,|\,\Phi\!>, \tag{18}$$

which can be used as accuracy checks in numerical calculations. In the multiplicative TIMF functional [1]

$$F'(\Phi,\Phi') = \frac{<\Phi'\,|\,\chi\!><\chi'\,|\,\Phi\!>}{<\Phi'\,|\,(E-\mathcal{H})\,|\,\Phi\!>}, \tag{19}$$

normalization factors of Φ, Φ' are irrelevant. With two–particle Slater determinants as trial functions

$$\begin{aligned} |\,\Phi\!> &= |\,\varphi_1\varphi_2\!> = \frac{1}{\sqrt{2}}\left[|\varphi_1\varphi_2) - |\varphi_2\varphi_1)\right], \\ <\Phi'\,| &= <\varphi_1'\varphi_2'\,| = \frac{1}{\sqrt{2}}\left[(\varphi_1'\varphi_2'| - (\varphi_2'\varphi_1'|\right], \end{aligned} \tag{20}$$

where straight, nonantisymmetrized products are denoted by round brackets $|\cdots)$, we find for the $(E-\mathcal{H})$–term in the above model

$$
\begin{aligned}
&<\Phi'\,|\,(E-\mathcal{H})\,|\,\Phi>= \\
&\quad E\,[<\varphi_1'\,|\,\varphi_1><\varphi_2'\,|\,\varphi_2> - <\varphi_1'\,|\,\varphi_2><\varphi_2'\,|\,\varphi_1>] \\
&\quad -\frac{1}{4}\Big[<\varphi_1'\,|\,q_1^2\,|\,\varphi_1> <\varphi_2'\,|\,\varphi_2>+ <\varphi_2'\,|\,q_2^2\,|\,\varphi_2> <\varphi_1'\,|\,\varphi_1> \\
&\quad - <\varphi_1'\,|\,q_1^2\,|\,\varphi_2> <\varphi_2'\,|\,\varphi_1>- <\varphi_2'\,|\,q_2^2\,|\,\varphi_1> <\varphi_1'\,|\,\varphi_2>\Big] \\
&\quad +\frac{1}{2}\,[<\varphi_1'\,|\,q_1\,|\,\varphi_1><\varphi_2'\,|\,q_2\,|\,\varphi_2> - <\varphi_1'\,|\,q_1\,|\,\varphi_2><\varphi_2'\,|\,q_2\,|\,\varphi_1>] \\
&\quad - <\varphi_1'\varphi_2'\,|\,v\,|\,\varphi_1\varphi_2>,
\end{aligned}
\tag{21}
$$

with $\mathcal{V}=v_{12}=v$. The terms in (17) leading to the inhomogeneities in the variational equations read

$$
<\Phi'\,|\,\chi> + <\chi'\,|\,\Phi> = <\varphi_1'\varphi_2'\,|\,\chi_{(+k)}\chi_{(-k)}> + <\chi_{(+k)}\chi_{(-k)}\,|\,\varphi_1\varphi_2>. \tag{22}
$$

The TIMF equations simplify when using the symmetries of the channel wave functions $\chi_{(+k)}$, $\chi_{(-k)}$ in the ansatz for the trial functions φ_1 and φ_2. According to (5) and (6), the functions $\chi_{(\pm k)}=\chi'_{(\pm k)}$ transform under the parity operator P and the antiunitary operator A of complex conjugation in the momentum representation as

$$
P\chi_{(+k)} = \chi_{(-k)}, \qquad P\chi_{(-k)} = \chi_{(+k)}, \tag{23}
$$

$$
A\chi_{(+k)} = \chi'_{(+k)} = \chi_{(+k)}, \qquad A\chi_{(-k)} = \chi'_{(-k)} = \chi_{(-k)}. \tag{24}
$$

With respect to the parity group Z_2 there exist the irreducible subspaces

$$
\chi_1 = \chi_1' = \frac{1}{\sqrt{2}}(\chi_{(+k)} + \chi_{(-k)}), \tag{25}
$$

$$
\chi_2 = \chi_2' = \frac{1}{\sqrt{2}}(\chi_{(-k)} - \chi_{(+k)}), \tag{26}
$$

with

$$
P\chi_1 = \chi_1 \quad , \quad P\chi_2 = -\chi_2 \ , \tag{27}
$$

and

$$
A\chi_1 = \chi_1' = \chi_1 \quad , \quad A\chi_2 = \chi_2' = \chi_2 \ . \tag{28}
$$

Because of the properties of Slater determinants it is clear that

$$|\,\chi_{(+k)}\chi_{(-k)}\!>\, = \,|\,\chi_1\chi_2\!>. \tag{29}$$

The commutation relations

$$\begin{aligned}
Pq_i^2 &= q_i^2 P, && (30)\\
(P\otimes P)(q_1\otimes q_2) &= (q_1\otimes q_2)(P\otimes P), && (31)\\
(P\otimes P)v &= v(P\otimes P), && (32)\\
Aq_i^2 &= (q_i^2)^+ A = q_i^2 A, && (33)\\
(A\otimes A)(q_1\otimes q_2) &= (q_1\otimes q_2)^+(A\otimes A) = (q_1\otimes q_2)(A\otimes A), && (34)\\
(A\otimes A)v &= v^+(A\otimes A) = v(A\otimes A), && (35)
\end{aligned}$$

where v^+, q^+ indicates hermitian conjugates, allow an ansatz, in the sense of a projection before variation, with trial functions of defined parity according to (27) and (28)

$$\begin{aligned}
P\varphi_1 &= \varphi_1, & P\varphi_2 &= -\varphi_2\,, && (36)\\
P\varphi_1' &= \varphi_1', & P\varphi_2' &= -\varphi_2'\,, && (37)\\
A\varphi_1 &= \varphi_1', & A\varphi_2 &= \varphi_2'\,. && (38)
\end{aligned}$$

This ansatz is self–consistent [4, 5]. One may note that in spite of $\chi_i = \chi_i'$ we have

$$\varphi_i(q) = \varphi_i'^*(q) \neq \varphi_i'(q) \tag{39}$$

because the complex energy leads to complex $\varphi_i(q)$, $\varphi_i'(q)$ even if the $\chi_i(q)$ are real. The choice (36) and (37) is preferred to the other possibility $\varphi_1 = P\varphi_2$ according to (23) because the parity of the trial functions leads to $<\varphi_1'\,|\,\varphi_2> \,=\, <\varphi_2'\,|\,\varphi_1> \,= 0$ and $<\varphi_i'\,|\,q_i\,|\,\varphi_i> \,= 0$ which simplifies (21) into

$$\begin{aligned}
&<\Phi'\,|\,(E-\mathcal{H})\,|\,\Phi>= && (40)\\
&\quad E\,[<\varphi_1'\,|\,\varphi_1><\varphi_2'\,|\,\varphi_2>]\\
&\quad -\frac{1}{4}\left[<\varphi_1'\,|\,q_1^2\,|\,\varphi_1>\,<\varphi_2'\,|\,\varphi_2>+\,<\varphi_2'\,|\,q_2^2\,|\,\varphi_2>\,<\varphi_1'\,|\,\varphi_1>\right]\\
&\quad +\frac{1}{2}\,[-<\varphi_1'\,|\,q_1\,|\,\varphi_2><\varphi_2'\,|\,q_2\,|\,\varphi_1>]\\
&\quad -<\varphi_1'\varphi_2'\,|\,v\,|\,\varphi_1\varphi_2>\,.
\end{aligned}$$

The functional derivatives with respect to $<\varphi_i'\,|$ follow immediately as

$$\frac{\delta <\Phi'\,|\,(E-\mathcal{H})\,|\,\Phi>}{\delta<\varphi_1'\,|} = \tag{41}$$
$$<\varphi_2'\,|\,\varphi_2>\left[E-\frac{1}{4}q_1^2-\frac{1}{4}\frac{<\varphi_2'\,|\,q_2^2\,|\,\varphi_2>}{<\varphi_2'\,|\,\varphi_2>}\right]|\,\varphi_1>$$
$$+ <\cdot\,\varphi_2'\,|\,(\frac{1}{2}q_1q_2-v)\,|\,\varphi_1\varphi_2> \;,$$

and

$$\frac{\delta <\Phi'\,|\,(E-\mathcal{H})\,|\,\Phi>}{\delta<\varphi_2'\,|} = \tag{42}$$
$$<\varphi_1'\,|\,\varphi_1>\left[E-\frac{1}{4}q_2^2-\frac{1}{4}\frac{<\varphi_1'\,|\,q_1^2\,|\,\varphi_1>}{<\varphi_1'\,|\,\varphi_1>}\right]|\,\varphi_2>$$
$$+ <\varphi_1'\,\cdot\,|\,(\frac{1}{2}q_1q_2-v)\,|\,\varphi_1\varphi_2>,$$

as well as for the inhomogeneous terms

$$\begin{aligned}\frac{\delta<\Phi'\,|\,\chi>}{\delta<\varphi_1'\,|} &= |\,\chi_{(+k)}><\varphi_2'\,|\,\chi_{(-k)}>-|\,\chi_{(-k)}><\varphi_2'\,|\,\chi_{(+k)}> \\ &= |\,\chi_1><\varphi_2'\,|\,\chi_2>,\end{aligned} \tag{43}$$

and

$$\begin{aligned}\frac{\delta<\Phi'\,|\,\chi>}{\delta<\varphi_2'\,|} &= |\,\chi_{(-k)}><\varphi_1'\,|\,\chi_{(+k)}>-|\,\chi_{(+k)}><\varphi_1'\,|\,\chi_{(-k)}> \\ &= |\,\chi_2><\varphi_1'\,|\,\chi_1>.\end{aligned} \tag{44}$$

We thus find the mean field equation for the orbital φ_1

$$\begin{aligned}&\left[<\varphi_2'\,|\,\varphi_2>\left(E-\frac{1}{4}q^2\right)-\frac{1}{4}<\varphi_2'\,|\,q^2\,|\,\varphi_2>\right]\varphi_1(q) \\ &-\frac{1}{2}\int dq'\;[q'\varphi_2(q')q\varphi_2(q)+w_2(q,q')]\,\varphi_1(q') \\ &= \chi_1(q)\,<\varphi_2'\,|\,\chi_2>\end{aligned} \tag{45}$$

with the self–consistent mean field potential

$$\begin{aligned}w_2(q,q') = -\lambda\nu^2\int dk\,dk'\,\delta(q+k-q'-k')(q-k)(q'-k') \\ \times\varphi_2(k)\varphi_2(k')\exp\left[-\frac{1}{4}\nu^2(q-k)^2\right]\exp\left[-\frac{1}{4}\nu^2(q'-k')^2\right],\end{aligned} \tag{46}$$

because the direct term gives the same contribution as the exchange term. The equation for φ_2 has the form

$$\begin{aligned}
&\left[<\varphi_1' \,|\, \varphi_1> \left(E - \frac{1}{4} q^2 \right) - \frac{1}{4} <\varphi_1' \,|\, q^2 \,|\, \varphi_1> \right] \varphi_2(q) \\
&\quad - \frac{1}{2} \int dq' \, \left[q' \varphi_1(q') q \varphi_1(q) + w_1(q,q') \right] \varphi_2(q') \\
&\quad = \chi_2(q) \, <\varphi_1'(q) \,|\, \chi_1(q)> \qquad (47)
\end{aligned}$$

with the self–consistent potential

$$\begin{aligned}
w_1(q,q') = -\lambda \nu^2 \int dk \, dk' \, \delta(q + k - q' - k')(q - k)(q' - k') \qquad (48) \\
\times \varphi_1(k) \varphi_1(k') \exp \left[-\frac{1}{4} \nu^2 (q-k)^2 \right] \exp \left[-\frac{1}{4} \nu^2 (q'-k')^2 \right].
\end{aligned}$$

After discretization of the variable q, the $\varphi_i(q)$ become vectors $\vec{\varphi}_i$, and the $\chi_i(q)$ become vectors $\vec{\chi}_i$. Then Eqs.(45), (47) read as matrix equations of the form $\mathbf{A}_i \vec{\varphi}_i = \vec{\chi}_i$ which have to be solved self–consistently. In a TIMF calculation we start with a first guess of the trial functions φ_i to find the integrals

$$<\varphi_i' \,|\, q^2 \,|\, \varphi_i> \;=\; \int dq \, \varphi_i(q)^2 q^2, \qquad (49)$$

$$<\varphi_i' \,|\, \varphi_i> \;=\; \int dq \, \varphi_i(q)^2, \qquad (50)$$

$$<\varphi_i' \,|\, \chi_i> \;=\; \int dq \, \varphi_i(q) \chi_i(q), \qquad (51)$$

as well as the self–consistent potentials $w_i(q,q')$. This defines the matrices $\mathbf{A}_i$, and then the inversion of the matrix equations yields new orbitals φ_i. These steps have to be repeated until convergence is reached.

The details of the iteration procedure can be chosen in different ways. For example, Eqs.(45), (47) can be implemented in a form with no direct coupling between φ_1 and φ_2 within a given iteration step n but with a term nonlocal with respect to the trial functions, for example in (45)

$$\int dq' \, \left[q \varphi_2^{(n-1)}(q) q' \varphi_2^{(n-1)}(q') \right] \varphi_1^{(n)}(q'). \qquad (52)$$

Of course, the trial functions are always coupled through the self–consistent quantities inherent in the equations. Another possibility would be updating the orbitals during iteration inside the above term according to

$$\varphi_2^{(n)}(q)\left[q\int dq'\,q'\varphi_2^{(n-1)}(q')\varphi_1^{(n-1)}(q')\right], \tag{53}$$

which is written as local with respect to $\varphi_2^{(n)}$. On the other hand, this introduces a direct coupling between $\varphi_1^{(n)}$ and $\varphi_2^{(n)}$, because this term is part of the equation for $\varphi_1^{(n)}$. We will use the first possibility with trial functions not directly coupled as indicated in (45), (47). This seems rather natural for the considered model, but the different possibilities have not yet been investigated systematically and the optimal way may depend on the time and storage resources of the actual computer to be used.

As a starting point for the iteration we need initial trial functions $\varphi_1^{(0)}$ and $\varphi_2^{(0)}$ which lie in the basin of attraction of a physically meaningful solution. Normally the basin of attraction is not known and it seems difficult to find good starting functions. In general, the problem is tackled by introducing additional parameters to form a problem where one knows the mean field solutions. Then one changes the additional parameters slowly to the physical values of the original problem. This is done while using the obtained mean field solutions as initial wave functions for the new, slightly changed parameters, hoping that one does not leave the basin of attraction. In the calculation of matrix elements of $\mathcal{G}$ it has been shown in Ref.[6] that TIMF becomes exact for $\mathrm{Im}(E)\to\infty$ with the solution $\varphi_i=\chi_i/E$. Thus, we begin with a large imaginary part of the energy and $\varphi_1^{(0)}=\chi_1/E$, $\varphi_2^{(0)}=\chi_2/E$ as starting orbitals. Then we diminish the imaginary part of the energy continuously until we reach the real axis at the desired point. This procedure has been tested with success [6, 7, 8] and no bifurcations, sudden loss of the solution or other disturbing effects occurred during iteration, if changes in parameter space are done slowly enough. Choosing one such path in the E–plane is equivalent to the choice of one solution branch for the nonlinear equations, out of possibly many ones.

An important feature of the TIMF solutions in these previous studies is the fact that the on–shell limes $\mathrm{Im}(E)\to 0$ has been fairly simple and that the self–energies remain complex even when $\mathrm{Im}(E)\to 0$. This is in contrast with the exact solution which becomes numerically more involved in that limit, if available at all [8]. The same holds for the present model. On one hand, for the numerical solution of the TIMF equations for the present model a mesh with 35 equidistant points on the one–dimensional q–axis was sufficient in all cases of the parameter ranges under study, even on–shell. On the other hand, for the exact solution this number of mesh points was not enough for the numerical evaluation of the integrals necessary even for moderate imaginary parts of the energy. For the on–shell limes we had to use automatic adaptive integration routines which use several hundred points for function evaluation. The TIMF solutions normally "remember" their origin from the square integrable starting functions χ_i/E and do not tend to develop peaks or sharp fine structures which are numerically difficult to handle.

The center–of–mass term complicates the numerical procedure. This term decreases for increasing particle number and is therefore usually skipped for large particle numbers or replaced by a constant. For only two particles, however, as in our model, this term is not small and has to be retained in the Hamiltonian of the model. It contributes as a strong, long ranged two–body operator and tends to destroy the convergence on the way towards the real energy axis due to sharp peaks of the wave functions creeping in, which are numerically disastrous. Convergence is thus quite difficult to obtain but can nonetheless be achieved by introducing an auxiliary parameter $\lambda_{c.m.}$ which swiches off the center–of–mass term at the beginning of the iteration and turns it on again slowly, parallel to the change in the imaginary part of energy. Combined with a relaxation method, where the new orbitals are mixed only partially to the old orbitals after every iteration, this leads to convergence if the parameters of this procedure are adjusted carefully. Typically, some hundred iterations have been necessary to come close enough to the real axis to obtain a good on–shell extrapolation. The problem is demonstrated in Figs.1 and 2 which show the two orbitals φ_1 and φ_2 beginning from an arbitrary iteration number for every fifth iteration step. One recognizes the similarity to χ_1 or χ_2, respectively, at the beginning and the growing peaks at the end. The stepwise growth of the peaks is due to the stepwise change of $\mathrm{Im}(E)$ and of the auxilliary parameter $\lambda_{c.m.}$ during iteration.

5 Inhomogeneous RPA (IRPA)

The inhomogeneous equation (9) for the present model,

$$(E - \mathcal{T} - \mathcal{V} + \mathcal{H}_{c.m.})|\,\Psi> = |\,\chi>, \tag{54}$$

is equivalent to the following homogeneous equation

$$(E-\mathcal{T}-\mathcal{V}+\mathcal{H}_{c.m.}-\Lambda|\,\chi><\chi\,|)|\,\Psi> = (E-\mathcal{H}')|\,\Psi> = 0. \tag{55}$$

Here we have introduced the nonhermitian Hamiltonian

$$\mathcal{H}' = \mathcal{T}+\mathcal{V}-\mathcal{H}_{c.m.}+\Lambda|\,\chi><\chi\,| \text{ with } \Lambda = \frac{1}{<\chi\,|\,\Psi>}. \tag{56}$$

In mean field approximation, (55) yields the generalized Hartree–Fock single–particle Hamiltonian

$$h' = h + \bar{\eta}\sum_{i=1}^{2}\frac{<\varphi_i'\,|\,\varphi_i>}{<\varphi_i'\,|\,\chi_i><\chi_i\,|\,\varphi_i>}|\,\chi_i><\chi_i\,|, \tag{57}$$

with the i–independent self–energy [1]

$$\bar{\eta} = E - \frac{<\Phi'\,|\,\mathcal{H}\,|\,\Phi>}{<\Phi'\,|\,\Phi>}. \tag{58}$$

This one–body operator is self–consistently defined with respect to the hole orbitals φ_i, φ_i'

$$<\varphi_i'\,|h' = <\varphi_i'\,|\eta_i, \quad h'|\,\varphi_i> = \eta_i|\,\varphi_i>, \tag{59}$$

and has particle orbitals φ_n, φ_n' as additional eigenfunctions

$$<\varphi_n'\,|h' = <\varphi_n'\,|\eta_n, \quad h'|\,\varphi_n> = \eta_n|\,\varphi_n>. \tag{60}$$

The biorthogonal creation and annihilation operators $a_i^\dagger$, a_i, $a_n^\dagger$, and a_n which correspond to the hole and particle orbitals φ_i, φ_i' and φ_n, φ_n', respectively, of this self–consistent single–particle Hamiltonian h' enable us to write the nonhermitian RPA ansatz [1]

$$Q_\nu^\dagger = \sum_{ni}\left(X_{ni}^\nu a_n^\dagger a_i - Y_{ni}^\nu a_i^\dagger a_n\right), \tag{61}$$

$$Q_\nu = \sum_{ni}\left(U_{ni}^\nu a_i^\dagger a_n - V_{ni}^\nu a_n^\dagger a_i\right). \tag{62}$$

Then two alike IRPA equations follow for the vectors $\binom{X^\nu}{Y^\nu}$ and $\binom{V^\nu}{U^\nu}$

$$\begin{pmatrix} A & B \\ C & D \end{pmatrix}\begin{pmatrix} X^\nu \\ Y^\nu \end{pmatrix} = (E_\nu - E)\begin{pmatrix} 1 & 0 \\ 0 & -1 \end{pmatrix}\begin{pmatrix} X^\nu \\ Y^\nu \end{pmatrix}, \tag{63}$$

$$\begin{pmatrix} A & B \\ C & D \end{pmatrix}\begin{pmatrix} V^\nu \\ U^\nu \end{pmatrix} = (E_\nu - E)\begin{pmatrix} 1 & 0 \\ 0 & -1 \end{pmatrix}\begin{pmatrix} V^\nu \\ U^\nu \end{pmatrix}, \tag{64}$$

with the coefficient matrices

$$A_{minj} = <\Phi' \,|\, [a_i^\dagger a_m, [\mathcal{H}', a_n^\dagger a_j]_-]_- \,|\, \Phi>, \tag{65}$$
$$B_{minj} = - <\Phi' \,|\, [a_i^\dagger a_m, [\mathcal{H}', a_j^\dagger a_n]_-]_- \,|\, \Phi>, \tag{66}$$
$$C_{minj} = - <\Phi' \,|\, [a_m^\dagger a_i, [\mathcal{H}', a_n^\dagger a_j]_-]_- \,|\, \Phi>, \tag{67}$$
$$D_{minj} = <\Phi' \,|\, [a_m^\dagger a_i, [\mathcal{H}', a_j^\dagger a_n]_-]_- \,|\, \Phi> . \tag{68}$$

Here i, j stand for holes and n, m for particles. and the the dimension of the matrices A, B, C, and D will be denoted by d.

The fact that the two Eqs.(63), (64) have the same form leads to the problem of dividing the $2d$ solutions into d solutions $\binom{X^\nu}{Y^\nu}$ and d solutions $\binom{V^\nu}{U^\nu}$, as discussed in [1]. In a hermitian RPA, eigenvectors with positive eigenvalues $\omega_\nu = (E_\nu - E)$ are selected as $\binom{X^\nu}{Y^\nu}$ to get an approximation for a (ground) state of minimal energy, while eigenvectors with negative ω_ν are denoted by $\binom{V^\nu}{U^\nu}$. In a nonhermitian RPA, where we have complex eigenvalues, the grouping can be done according to the imaginary part of the eigenvalues, where the $\binom{X^\nu}{Y^\nu}$ have eigenvalues with Im $\omega_\nu < 0$. Alternatively, we can identify the $\binom{X^\nu}{Y^\nu}$ by starting from a Tamm–Dancoff approximation (TDA), i.e. setting $B = C = 0$. Then $Y = V = 0$ and X is determined by $AX^\nu = \omega_\nu A^\nu$. Then we can follow the solutions by slowly switching on B and C.

Having selected the $\binom{X^\nu}{Y^\nu}$ one can calculate the RPA energy correction as

$$\Delta E = \frac{1}{2} \left(\mathrm{Tr}\, \omega - \mathrm{Tr}\, A \right), \tag{69}$$

where ω is the matrix of eigenvalues of the $\binom{X^\nu}{Y^\nu}$ only.

Writing down the IRPA equations for the present model one can make use of the symmetries of the problem. The bra–ket symmetry (28) with the ansatz (38) yields

$$<\chi_i \,|\, \varphi_j> = <\varphi'_j \,|\, \chi_i>. \tag{70}$$

Furthermore, the occurring two–body operators fulfil the relations

$$<\varphi'_m \varphi'_n \,|\, v \,|\, \varphi_i \varphi_j> = <\varphi'_i \varphi'_j \,|\, v \,|\, \varphi_m \varphi_n>, \tag{71}$$
$$-\frac{1}{2} <\varphi'_m \varphi'_n \,|\, q_1 q_2 \,|\, \varphi_i \varphi_j> = -\frac{1}{2} <\varphi'_i \varphi'_j \,|\, q_1 q_2 \,|\, \varphi_m \varphi_n>, \tag{72}$$

where the indices m, n stand for particles and i, j for holes. Denoting the sum of both two–body operators $\mathcal{V}$ and $-q_1q_2/2$ by w we have $w_{m'n'ij} = w_{i'j'mn}$ and, analogously, $w_{m'j'in} = w_{n'i'jm}$. With those relations we have the following expressions for the IRPA matrices A, B, C, D [1]

$$\begin{aligned} A_{minj} &= \delta_{ij}\left(t_{m'n} + \sum_{l=1}^{N} w_{m'l'nl}\right) - \delta_{nm}\left(t_{j'i} + \sum_{l=1}^{N} w_{j'l'il} + \delta_{ij}\bar{\eta}\right) \\ &\quad + w_{m'j'in} + \bar{\eta}\, \frac{<\varphi'_m\,|\,\chi_i><\chi_j\,|\,\varphi_n>}{<\varphi'_i\,|\,\chi_i><\chi_j\,|\,\varphi_j>}, \qquad (73) \\ B_{minj} &= w_{m'n'ij} + \bar{\eta}\frac{<\varphi'_m\varphi'_n\,|\,\chi_i\chi_j>}{<\varphi'_i\,|\,\chi_i><\varphi'_j\,|\,\chi_j>}, \qquad (74) \\ C_{minj} &= w_{i'j'mn} + \bar{\eta}\frac{<\chi_i\chi_j\,|\,\varphi_m\varphi_n>}{<\chi_i\,|\,\varphi_i><\chi_j\,|\,\varphi_j>}, \qquad (75) \\ D_{minj} &= A_{njmi}, \qquad (76) \end{aligned}$$

and can verify the relations

$$B = C \quad , \quad A = \tilde{A} \qquad (77)$$

besides the general symmetries $A = \tilde{D}$, $B = \tilde{B}$, $C = \tilde{C}$ [1]. The IRPA matrix M becomes

$$M = \begin{pmatrix} A & B \\ C & D \end{pmatrix} = \begin{pmatrix} A & B \\ B & A \end{pmatrix}. \qquad (78)$$

Because $B = \tilde{B}$ holds, this means

$$M = \tilde{M}, \qquad (79)$$

and together with $\tilde{M} = \gamma M \gamma$ follows

$$M = \gamma M \gamma. \qquad (80)$$

From the existence of a right eigenvector $v^\nu = \binom{X^\nu}{Y^\nu}$ to the IRPA equation with eigenvalue ω_ν,

$$\eta M v^\nu = \omega_\nu v^\nu, \qquad (81)$$

follows the existence of a left eigenvector $(Y^\nu, -X^\nu)$ with eigenvalue $-\omega_\nu$ [1]. Because of relation (80) one finds, using $\eta\gamma = -\gamma\eta$ and $\gamma^2 = 1$,

$$\begin{aligned} \eta M v^\nu &= \eta\gamma M \gamma v^\nu = -\gamma\eta M \gamma v^\nu \\ \Rightarrow\; -\eta M \gamma v^\nu &= \gamma\omega_\nu v^\nu \\ \Rightarrow\; \eta M(\gamma v^\nu) &= -\omega_\nu(\gamma v^\nu). \qquad (82) \end{aligned}$$

This means that there exists a right eigenvector

$$\gamma v^\nu = \begin{pmatrix} Y^\nu \\ X^\nu \end{pmatrix} \tag{83}$$

with eigenvalue $-\omega_\nu$ which we identify with $\binom{V^\nu}{U^\nu}$ from (64). In this way the additional symmetries (77) lead to

$$Y = V, \quad X = U \tag{84}$$

which is equivalent to

$$\gamma T \gamma = T \quad \text{or} \quad T\eta\tilde{T}\eta = 1, \tag{85}$$

in contrast with unitary canonical transformations which obey $Y^* = V, X^* = U$, and therefore $T\eta T^+\eta = 1$. The resulting symmetry relation (83) between eigenvector v^ν belonging to eigenvalue ω_ν and eigenvector γv^ν belonging to eigenvalue $-\omega_\nu$ can be used as a consistency check in numerical calculations.

Keeping in mind that the center–of–mass term $-\frac{1}{2}q_1 q_2$ contributes to the matrix elements $w_{m'n'ij}$ and $w_{m'j'in}$, one can write the matrices for the IRPA equations of the model as

$$\begin{aligned}
A_{minj} &= \delta_{ij}\delta_{nm}(\eta_n - \eta_i) - \delta_{ij}\bar{\eta}\sum_{l=1}^{2}\frac{<\varphi'_m\,|\,\chi_l><\chi_l\,|\,\varphi_n>}{<\varphi'_l\,|\,\chi_l><\chi_l\,|\,\varphi_l>} \\
&\quad + <\varphi'_m\varphi'_j\,|\,v\,|\,\varphi_i\varphi_n> -\frac{1}{2}<\varphi'_m\varphi'_j\,|\,q_1 q_2\,|\,\varphi_i\varphi_n> \\
&\quad + \bar{\eta}\frac{<\varphi'_m\,|\,\chi_i><\chi_j\,|\,\varphi_n>}{<\varphi'_i\,|\,\chi_i><\chi_j\,|\,\varphi_j>}, \qquad (86) \\
B_{minj} &= <\varphi'_m\varphi'_n\,|\,v\,|\,\varphi_i\varphi_j> -\frac{1}{2}<\varphi'_m\varphi'_n\,|\,q_1 q_2\,|\,\varphi_i\varphi_j> \\
&\quad + \bar{\eta}\frac{<\varphi'_m\varphi'_n\,|\,\chi_i\chi_j>}{<\varphi'_i\,|\,\chi_i><\varphi'_j\,|\,\chi_j>}, \qquad (87)
\end{aligned}$$

using the particle and hole eigenvalues η_i and η_n of h'.

The whole IRPA procedure can be described as follows

1. One starts with a TIMF approximation at the desired energy E.

2. This defines the corresponding Hartree–Fock operator h' for $\mathcal{H}'$.

3. The diagonalization of h' gives the particle orbitals φ_n. The maximal number of possible particle orbitals obtained depends on the number of mesh points. (This step will be discussed again in the next section.)

4. Solving the IRPA equation with all these orbitals or a subset of them gives the IRPA eigenvalues.

5. By comparison with a TDA and continuity or, alternatively, by the sign of the imaginary part those eigenvalues are selected which contribute to the energy correction $(\Delta E)_1$.

6. The energy correction is used to give a guess for a new energy E_1 such that $E_1 + (\Delta E)_1 \approx E$. With this new energy E_1 but with all other parameters unchanged, including the boost k, one goes back to step 1. This procedure is repeated until, after p passes, the IRPA energy $E_p + (\Delta E)_p$ is equal to the desired energy E.

For the last step we stress that the boost of the χ_i has to be kept constant during the iteration. That is due to the aim of calculating the amplitude D for given (i.e. fixed) channel wave functions. Having found the energy correction which leads to the desired energy E means that the TIMF value of the amplitude $D_{TIMF}(E_p)$ for the shifted energy E_p is the IRPA approximation $D_{IRPA}(E)$ for the energy E. This result can be compared with the TIMF solution $D_{TIMF}(E)$ directly for E.

6 IRPA with Square Integrable Particle Orbitals (SIRPA)

Trying a direct numerical implementation of the above procedure leads to a problem related to the continuous spectrum. The particle orbitals constructed from the Hartree–Fock operator h' show a numerically undesirable characteristic. They are nearly fully concentrated on single mesh points which represent a discrete analogy of δ–functions in momentum space and of plane waves in coordinate space. Only the bound state created by the separable potential $\mathcal{V}$ is an exception. This is not surprising, because the additional separable term consisting of the square integrable χ_i genererates $n = 2$ square integrable hole orbitals as eigenfunctions of h', but the remaining eigenfunctions cannot deny their origin from the continuous $\mathcal{H}'$–spectrum. This is exemplified in Figs.3 and 4. They show the eigenfunctions of the Hartree–Fock Hamiltonian h' for a specific choice of parameters. With a lattice of 35 points there are 35 eigenfunctions with positive and negative parities, respectively. The peaks of the negative parity orbitals pointing downwards are concealed behind the drawing plane. Such orbitals make the IRPA results unstable with respect to changes of the mesh and are therefore useless for numerical applications.

For large enough Λ and square integrable χ, χ' the hole orbitals become square integrable by the $\Lambda|\,\chi><\chi'\,|$–term even in the absence of a potential in $\mathcal{H}$. One might argue whether more separable terms could do the same for particle orbitals. Such additional terms in $\mathcal{H}'$ would be admissible only if they do not change the exact solutions Ψ, Ψ' of (55). But the exact solutions are at best known approximately, which means that additional terms practically cannot be biorthogonalized with respect to these unknown solutions. If they are not exactly biorthogonal to Ψ, Ψ', then these solutions are no longer exact solutions of $\mathcal{H}'$ with the additional terms added. Only for the self–consistent one–body h' with known eigenfunctions such an addition of appropriate biorthogonalized separable one–body terms would be possible.

We can remedy the situation by realizing for what purpose we actually need the particle and hole operators. Besides their property of annihilating the bra or ket reference states, respectively, they are only needed to form a complete basis. And this is fulfilled by any complete biorthogonal system as long as it contains the holes unchanged and does not mix hole components into particle orbitals. It is not necessary that particle orbitals are eigenstates of h'. Without further difficulties it is therefore possible to replace the third step of the IRPA procedure by the selection of an arbitrary basis system of square integrable functions as particle orbitals which have to be biorthogonalized with respect to the hole orbitals. The IRPA equations have to be slightly modified for that purpose, because we cannot use anymore the fact that particle orbitals are eigenfunctions of h'. But this does not complicate calculations and gives rise to the important additional freedom of choosing the particle orbitals best suited for the problem. It will turn out that this is essential for numerical applications to the model. In the following, we call the inhomogeneous RPA using square integrable particle orbitals Square integrable Inhomogeneous RPA (SIRPA). An example of particle orbitals generated in such a way is given in Figs.5 and 6. They show, starting with the TIMF solutions φ_1, φ_2 (hole orbitals), eight additional square integrable φ_n, biorthogonalized to the bra–orbitals. These have been constructed by a Schmidt (bi)orthogonalization procedure starting with Gaussians as in (5) and (6) with differing boosts. For SIRPA the matrices A and B from (86) and (87) have to be recalculated using binormalized orbitals φ'_α, φ_α but no particle eigenenergies η_n

$$\begin{aligned}
A_{minj} &= \delta_{ij}\,(-\delta_{nm}\eta_i + <\varphi'_m\,|\,t\,|\,\varphi_n>) \\
&\quad +\delta_{ij}\sum_{l=1}^{2}\Big(<\varphi'_m\varphi'_l\,|\,v\,|\,\varphi_n\varphi_l> -\frac{1}{2}<\varphi'_m\varphi'_l\,|\,q_1q_2\,|\,\varphi_n\varphi_l>\Big) \\
&\quad +\ <\varphi'_m\varphi'_j\,|\,v\,|\,\varphi_i\varphi_n> -\frac{1}{2}<\varphi'_m\varphi'_j\,|\,q_1q_2\,|\,\varphi_i\varphi_n> \\
&\quad +\bar{\eta}\frac{<\varphi'_m\,|\,\chi_i><\chi_j\,|\,\varphi_n>}{<\varphi'_i\,|\,\chi_i><\chi_j\,|\,\varphi_j>}, \qquad (88)\\
B_{minj} &= <\varphi'_m\varphi'_n\,|\,v\,|\,\varphi_i\varphi_j> -\frac{1}{2}<\varphi'_m\varphi'_n\,|\,q_1q_2\,|\,\varphi_i\varphi_j> \\
&\quad +\bar{\eta}\frac{<\varphi'_m\varphi'_n\,|\,\chi_i\chi_j>}{<\varphi'_i\,|\,\chi_i><\varphi_j\,|\,\chi_j>}. \qquad (89)
\end{aligned}$$

Here one recognizes that inside the terms with the $\bar{\eta}$–factor only the overlaps of the particle states with the channel wave functions $<\varphi'_n\,|\,\chi_i>$ and $<\chi_i\,|\,\varphi_n>$ contribute. Therefore, we construct particle orbitals φ_{χ_i}, φ'_{χ_i} from χ_i by biorthogonalization with respect to the holes φ_i, φ'_i. More particle orbitals cannot contribute to the terms with the $\bar{\eta}$–factor in (88), (89), because further particle orbitals are biorthogonal to φ_i, φ'_i, φ_{χ_i}, φ'_{χ_i} and therefore also to χ_i. Further particle orbitals can enter the equations only through the two–body operators $\mathcal{V}$ and $-q_1q_2/2$ but not through the mean field terms arising from $\Lambda|\,\chi><\chi\,|$. We expect therefore that the particle orbitals φ_{χ_i}, φ'_{χ_i} will give the main contribution to SIRPA and this is indeed confirmed by the following numerical studies. This possibility of restricting to only two particle orbitals in the present model is an essential practical improvement of SIRPA over IRPA.

To get a better idea of the SIRPA procedure we use a specific example as depicted in Figs.7 and 8. The figures show a cut from the surface generated by the real or imaginary parts of the exact amplitude over the energy plane for constant boost k. The $(+)$ sign denotes the TIMF estimate $D_{TIMF}(E_0) = 0.00291 - i0.2907$ (TIMF(old)) for the energy $E_0 = 6.25 + i2.0$. The broken line shows the deviation from the exact amplitude $D_{Exact}(E_0) = 0.00363 - i0.2937$ (Exact(old),$\diamond$) at that point. Now the SIRPA procedure gives an energy correction $(\Delta E)_1$ for fixed amplitude TIMF(old). Accordingly, the value of TIMF(old) is plotted again at energy $E_0' = E_0 + (\Delta E)_1 = 6.241 + i2.012$ and denoted by RPA(new) $(\times)$, because it is the SIRPA result $D_{SIRPA}(E_0')$ for this shifted energy. The deviation from the exact amplitude $D_{Exact}(E_0') = 0.00294 - i0.2929$ (Exact(new), $\Box$) at that new point is again indicated by a broken line and corresponds to the SIRPA error. As seen from the figures, this SIRPA error is quite small for the real part of D, and even for the imaginary part it is still smaller than the TIMF error. Additional information is contained in the figures by the value $D_{Min} = 0.00291 - i0.2907$ denoted as Exact(Min.) $(\triangle)$ at energy $E_{Min} = 6.243 + i2.045$. This point shows the amplitude with minimal deviation, in the sense of least squares, from the amplitude TIMF(old). As a deviation is not visible in the figures at the point $(\triangle\ )$, the value TIMF(old) equals an exact amplitude. One sees that the real part of the SIRPA energy is in good coincidence with the energy corresponding to the amplitude Exact(Min.), while the difference is larger for the imaginary part.

In the next step one has to find an energy E_i such that $E_i + (\Delta E)_i$ becomes equal to $E = E_0$. At first glance one might think that this can require a lengthy search, but in the present model it turns out to be sufficient in all cases to take

$$E_1 = E_0 - (\Delta E)_1. \tag{90}$$

Because the first energy correction $(\Delta E)_1$ is nearly equal to the second $(\Delta E)_2$, the following relation holds approximately

$$E_1 + (\Delta E)_2 = E_0 + (\,(\Delta E)_2 - (\Delta E)_1\,) \approx E_0. \tag{91}$$

This has been confirmed in the following calculations within our model.

Even the selection of the SIRPA eigenvalues needed for the evaluation of the energy correction

$$\Delta E = \frac{1}{2}\,(\mathrm{Tr}\,\omega - \mathrm{Tr}A)\,, \tag{92}$$

turns out to be quite simple. Because the SIRPA eigenvalues are not very different from the TDA eigenvalues, it was possible to select simply the SIRPA eigenvalues with smallest (absolute) distance to the TDA eigenvalues, instead of using a procedure of slowly going from TDA to SIRPA [1]. Additionally, the selected eigenvalues possess a negative imaginary part in all interesting regions, as desired. It follows that already the imaginary part of the eigenvalues allows the correct selection in our model.

Under these circumstances one has to solve the TIMF, TDA and SIRPA equations two times only to achieve the final result.

7 Numerical Results

The above model has been investigated over a large range of parameters. A lattice containing about 35 points, going for instance from $-7.0b$ to $7.0b$, has been found adequate for energies up to 6.25 [MeV], setting $\hbar^2/m = 1$. The factor λ of the potential has been varied, besides some negative values, between 0 and 20 but has normally been set to 1 as well as b and ν. The calculation of the exact, TIMF and SIRPA amplitudes proceeds as discussed in the former Sections. In most cases we worked with the two particle orbitals originating from χ_1, χ_2 only, as this turns out to be sufficient. Table 1 shows an example of SIRPA and TDA eigenvalues. One recognizes, besides the $\pm$–symmetry of the SIRPA eigenvalues, that the separation of the SIRPA eigenvalues into two groups can be done easily by comparison with the TDA values. Additionally, all TDA values have negative imaginary parts.

	Re	Im
TDA	-6.612514	-0.772935
	-6.229611	-0.850048
	-0.050423	-4.531350
	0.228851	-3.508958
SIRPA	-6.635630	-0.774979
	6.635630	0.774979
	-6.254120	-0.851742
	6.254120	0.851742
	-0.057787	-4.497871
	0.057787	4.497871
	0.222676	-3.465099
	-0.222676	3.465099

Table 1: TDA- and SIRPA-eigenvalues at Re(E)=6.25, Im(E)=0.8 and λ=1.

For a general orientation, Figs.9, 10, and 11, 12 display the landscape of the exact amplitude over the complex energy plane or in its dependence of the real part of energy and λ, respectively. The exact amplitude cannot be calculated for an exactly vanishing Im(E) and, therefore, the line Im(E) = 0 is not drawn in the figures. The step or kink, respectively, located at the real energy axis is clearly visible.

In the following, several typical results of the numerical calculations are presented. Tables 2 and 3 list the results of the successive steps of a SIRPA procedure for a typical set of parameter values. The first line of the tables shows the exact and TIMF amplitudes, $D_{Exact} = D_{Exact}(E_0)$ and $D_{TIMF} = D_{TIMF}(E_0)$, for a given energy E_0. The first SIRPA calculation yields a shifted energy $E_0' = E_0 + (\Delta E)_1$ for the amplitude D_{TIMF}. The second line shows again an exact and a TIMF amplitude, $D'_{Exact} = D_{Exact}(E_0')$ and $D'_{TIMF} = D_{TIMF}(E_0')$, but for the shifted energy E_0'. We already emphasized that the boost $k = (\mathrm{Re}(E_0))^{1/2}$ has to be kept constant for the shifted energy. Though not really necessary for the further calculations, this line already gives a very good approximation D^0_{SIRPA} to the final SIRPA amplitude D_{SIRPA} at E_0. Because the amplitude correction $\Delta D = D_{TIMF}(E_0) - D_{TIMF}(E_0')$ for E_0' is nearly independent of the small energy difference $(\Delta E)_1$, the amplitude

$$D^0_{SIRPA}(E_0) = D_{TIMF}(E_0) + \Delta D = 2\,D_{TIMF}(E_0) - D_{TIMF}(E_0') \qquad (93)$$

is a good approximation of $D_{SIRPA}(E_0)$. The third line shows, as a second step of the SIRPA procedure, the TIMF amplitude compared with the exact amplitude for the shifted energy $E_1 = E_0 - (\Delta E)_1$ and constant boost $k = (\mathrm{Re}(E_0))^{1/2}$. The SIRPA energy correction $(\Delta E)_2$ leads to the energy $E_1' = E_1 + (\Delta E)_2$ which agrees well with E_0. Thus, the TIMF amplitude in this line represents the SIRPA amplitude D_{SIRPA} for energy E_0 we were looking for,

$$D_{SIRPA}(E_0) = D_{TIMF}(E_1). \qquad (94)$$

As a check, the fourth line shows that for $E_1' = E_1 + (\Delta E)_2$ the first line is indeed reproduced almost perfectly. The small deviation in the real part of the amplitude in Table 2 indicates the possibility of a small improvement of the result by further iterations. The last lines of Tables 2 and 3 summarize the obtained results. For fixed $E = E_0$ the exact amplitude $D_{Exact}(E_0)$, the TIMF amplitude $D_{TIMF}(E_0)$, the SIRPA amplitude $D_{SIRPA}(E_0)$ and the one–step approximation of the latter, $D^0_{SIRPA}(E_0)$, are listed. The amplitude $D_{Min} = D_{Min}(E_{Min})$ is an actual value of the exact amplitude at energy E_{Min}, which deviates minimally in the sense of least squares from D_{SIRPA} in both real and imaginary parts. This shows that the amplitude D_{SIRPA} indeed occurs as an exact value for a shifted energy. Finally, one finds the TIMF and SIRPA errors in the Tables 2 and 3, absolute as well as relative to the exact amplitude. According to Table 2 (Table 3) the TIMF error for the real part relative to the exact amplitude is 19.79%(9.17%) and for the imaginary part 1.11%(1.79%). SIRPA reduces this error to 0.28%(0.29%) or 0.85%(1.41%), respectively, which clearly makes an improvement, especially for the real part.

	Energy		Exact Amplitude		TIMF	
	Re	Im	Re$\times 10^{-2}$	Im	Re$\times 10^{-2}$	Im
E_0	6.2500	1.8000	0.4988	-0.3076	0.4145	-0.3041
E_0'	6.2391	1.8127	0.4107	-0.3067	0.3295	-0.3033
E_1	6.2609	1.7873	0.5877	-0.3084	0.5002	-0.3050
E_1'	6.2499	1.8000	0.4985	-0.3076	0.4141	-0.3041
			Re$\times 10^{-2}$	Im		
E=E_0		D_{Exact}	0.4988	-0.3076		
		D^0_{SIRPA}	0.4995	-0.3049		
		D_{SIRPA}	0.5002	-0.3050		
		D_{TIMF}	0.4145	-0.3041	relat. error:	
		D_{Min}	0.5002	-0.3050	Re	Im
		$D_{TIMF} - D_{Exact}$	-0.0844	0.0034	19.79%	1.11%
		$D_{SIRPA} - D_{Exact}$	0.0014	0.0026	0.28%	0.85%
			Re	Im		
$D =$		E_{Min}	6.2539	1.8361		
D_{SIRPA}		E_{SIRPA}	6.2499	1.8000		
		E_{TIMF}	6.2609	1.7873		
		$E_{TIMF} - E_{Min}$	0.0070	-0.0487		
		$E_{SIRPA} - E_{Min}$	-0.0040	-0.0360		

Table 2: Results of a SIRPA-calculation at $\lambda = 1$, boost $= 2.5$ and Im $(E) = 1.8$

	Energy		Exact Amplitude		TIMF	
	Re	Im	Re	Im	Re	Im
E_0	6.2500	0.8000	0.01732	-0.3967	0.01580	-0.3896
E_0'	6.2374	0.8152	0.01567	-0.3953	0.01424	-0.3882
E_1	6.2626	0.7849	0.01899	-0.3981	0.01739	-0.3909
E_1'	6.2499	0.8000	0.01732	-0.3967	0.01580	-0.3896
			Re	Im		
E=E_0	D_{Exact}		0.01732	-0.3967		
	D^0_{SIRPA}		0.01736	-0.3910		
	D_{SIRPA}		0.01739	-0.3909		
	D_{TIMF}		0.01580	-0.3896	relat. error:	
	D_{Min}		0.01739	-0.3909	Re	Im
	$D_{TIMF} - D_{Exact}$		-0.00152	0.0071	9.17%	1.78%
	$D_{SIRPA} - D_{Exact}$		0.00005	0.0056	0.29%	1.41%
			Re	Im		
$D =$	E_{Min}		6.2596	0.8517		
D_{SIRPA}	E_{SIRPA}		6.2499	0.8000		
	E_{TIMF}		6.2626	0.7849		
	$E_{TIMF} - E_{Min}$		0.0030	-0.0669		
	$E_{SIRPA} - E_{Min}$		-0.0097	-0.0517		

Table 3: Results of a SIRPA-calculation at $\lambda = 1$, boost $= 2.5$ and Im $(E) = 0.8$

The last part of the two Tables takes another point of view. If we regard the procedure as a homogeneous, nonhermitian Hartree–Fock approximation we can compare for fixed $D = D_{SIRPA}$, which means fixed $\mathcal{H}'(\Lambda = 1/D_{SIRPA})$, the generalized Hartree–Fock(=TIMF) energy $E_{TIMF} = E_1$ with the generalized RPA(=SIRPA) energy $E_{SIRPA} = E_1' \approx E_0$ and a corresponding discrete, exact eigenenergy $E_{Exact}(D_{SIRPA})$ of $\mathcal{H}'$. We replace the energy $E_{Exact}(D_{SIRPA})$ by the energy E_{Min}, because for a given amplitude D which results from a TIMF calculation there need not exist an energy E for which the value D appears as exact amplitude in $D_{Exact}(E) = <\chi' \,|\, (E - \mathcal{H})^{-1} \,|\, \chi>$. If we consider, for instance, large amplitudes D, then $\Lambda = 1/D$ in $\mathcal{H}'$ might be too small to produce an additional square integrable eigenstate near the starting energy E_0. The situation is exemplified in Figs.13 and 14. They show, analogous to Figs.7 and 8, the landscape created over the complex E–plane by $D_{Exact}(E) = <\chi' \,|\, (E - \mathcal{H})^{-1} \,|\, \chi>$ for fixed χ, χ'. The contour lines give an impression of the curves of constant real or imaginary part of the amplitude, respectively. If we are searching for an energy where a given complex number D, i.e. in our case the approximation D_{TIMF} for some energy E_0, is the numerical value of an exact amplitude, we have to look for a common point of the two contour lines corresponding to fixed real part $\mathrm{Re}(D_{Exact}) = \mathrm{Re}(D)$ and imaginary part $\mathrm{Im}(D_{Exact}) = \mathrm{Im}(D)$. Only, if such a common point exists, say at energy E, we have $D_{Exact}(E) = D$ for both, real and imaginary part of the amplitudes, i.e. in our case $D_{Exact}(E) = D_{TIMF}(E_0)$, where E_0 will normally not be equal to E. This means, that besides the original $\mathcal{H}$–bound states, there exists another discrete eigenvalue $E(D)$ of $\mathcal{H}'(D)$. As one can see from the Figures for positive real part of energies, this is surely not the case for large D. This explains why we look for an energy E_{Min} where the exact amplitude D_{Min} is nearest in a least square sense to a given $D = D_{SIRPA}$ in both real and imaginary parts. To this end, we use a gradient search starting from the energy E_{SIRPA}. In our case, because of the smallness of the amplitude correction produced by SIRPA, the two contour lines of Figs.13, 14 have a common point as sketched in the following scheme

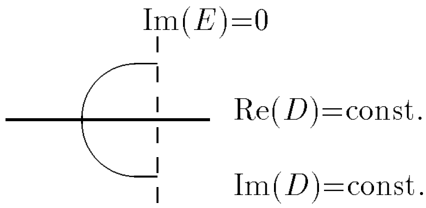

This is confirmed by the fact that D_{Min} only deviates from the given $D = D_{SIRPA}$ within the numerical tolerance and therefore the energy E_{Min} can be regarded here as the exact energy. The last three lines of Tables 2 and 3 take that homogeneous viewpoint and show the three energies E_{TIMF}, E_{SIRPA} and E_{Min}. One sees that the SIRPA energies interpolate between E_{Min} and E_{TIMF} for the imaginary part. For the real part E_{SIRPA} is nearer to E_{Min} compared to the TIMF energy in Table 2. In Table 3 the situation is reversed for the real part, i.e. the SIRPA energy is a worse approximation than the TIMF result. But even at this point the SIRPA approximation of the amplitude is still better than the TIMF value. Figs.15, 16 show the pole in the amplitude indicating the bound state of the separable potential which is not visible in Figs.13, 14 because of the scale used.

After these explanations of the SIRPA procedure we present the results of the numerical calculations graphically. In Figs.17, 18 the amplitudes for a variable real part of the energy and a fixed imaginary part are drawn. The improvement of SIRPA over TIMF is clearly seen over the whole parameter range: For the real part the SIRPA amplitude is close to the exact one while for the imaginary part the figure shows a slight improvement. Figs.19 and 20 display a larger energy range for the same curves. One notes that TIMF yields a good approximation to the exact amplitude. The improvement of SIRPA is difficult to see, because the total variation of the amplitude over the displayed Re(E)–range is large compared to the TIMF error and the SIRPA correction. The situation gets clearer in Figs.21 and 22. The former, Fig.21, shows the deviations of the TIMF and SIRPA results from D_{Exact}. One can see that the SIRPA values lie nearly everywhere closer to zero; the only exception is at the point where the TIMF curve crosses the zero line. In the neighborhood of this accidental crossing point, SIRPA cannot be better than TIMF, but the SIRPA error remains small there and the SIRPA curve turns out to be better than TIMF again on both sides close to that point. One may remark at this point that the region of small $\mathrm{Re}(E)$ is not very interesting, because on one hand the TIMF approximation gets better there because $\mathrm{Im}(E)$ is large relative to $\mathrm{Re}(E)$. On the other hand the overlap of the one–particle wave functions, boosted by $\pm k$, increases and the antisymmetric combination of these two tends to zero which makes them unsuitable as model channel wave functions.

One may ask why the small variation of the amplitude curves within the interval of the relativeley small SIRPA energy correction can produce such a considerable improvement of SIRPA results over TIMF. This is due to the fact that the SIRPA iteration is done with constant boost, though the energies change during iteration, and curves with constant boost show a much stronger variation than those with adapted boost (see Figs.7, 8).

The homogeneous point of view is taken again in Fig.22. As discussed in connection with Tables 2 and 3, one can compare for a fixed diagonal amplitude the three energies E_{TIMF}, E_{SIRPA} and E_{Min}, where E_{Min} can be regarded as the exact energy. Fig.22 shows the deviation of E_{TIMF} and E_{SIRPA} from E_{Min}. In this Figure one sees again that SIRPA does better than TIMF especially for not too small energies. Moreover, the point of intersection of the TIMF curve for the real part coincides with that one of the SIRPA curve. That means that even at that point SIRPA is not worse than TIMF.

Altogether, the above results show that SIRPA brings an improvement over TIMF for inverting operators in Fock space. For the selected case of calculation of $\mathcal{G}$ there remains the special question of the on–shell limit of energy. As discussed in connection with the TIMF calculation, this limit it not as easy as usual in the present model due to the difficulties of the TIMF procedure connected with the center–of–mass correction. But once this limit is reached for TIMF, no new problems arise for the SIRPA procedure which therefore can deal with this limit, if TIMF does. In general one can consider two cases:

1. The energy correction of SIRPA relative to TIMF points closer to the real energy axis. One has to stop the procedure, if the SIRPA energy lies on–shell.

2. The situation is more difficult if the SIRPA corrected energies points are farther off–shell compared to the TIMF energy. One can try to continue the TIMF calculations through the real energy axis to energies with negative imaginary part, if one is able to keep the TIMF solutions retarded. Again the limit is reached when the SIRPA energies are on–shell.

Because of on–shell convergence problems of TIMF we used for the present model a simpler procedure which can be applied to both cases. We calculate the amplitudes for several imaginary parts of the energy up to a point as close to the real axis as possible and extrapolate the resulting curves to real energies. For a fit of the curves we used polynomials or rational (Padé–)approximants of the form

$$f(x) = \frac{\sum_{i=0}^{n} a_i x^i}{1 + cx}, \tag{95}$$

where the coefficients a_i and c are determined by a least square criterion. Then an extrapolation to $\mathrm{Im}(E)$=0 is done. During the approximation, the polynomial degree n has been increased until all data points had been well fitted and the on–shell value had stabilized. This was possible before sharp oscillations in the fitting functions occurred, which are typical in approximation problems for large n. An example for a rational approximation function is shown in Figs.23 and 24. The drawn points represent the points used for the fit, while the lines show the fit functions and, for comparison, the curve of the exact amplitude. Again, because of the large variation of the amplitudes compared to their differences, Figs.25, 26 display only the interesting range near the real axis. One recognizes that the improvement of SIRPA is mainly for the real part of the amplitude while the imaginary part is only altered very little, but into the right direction. This phenomenon might be understood by the fact that TIMF calculates simultaneously real and imaginary part of the amplitude and yields a smaller relative error for the larger of the two numbers, which in our case is the imaginary part. Thus, SIRPA can be regarded as a method which diminishes the relatively large TIMF error for the real part of the amplitude and only slightly improves the good TIMF approximation for the imaginary part of the amplitude.

Figs.27 and 28 show, analogously to Figs.21 and 22, the deviations from the exact values. It may be noticed that SIRPA brings an improvement for the amplitudes even when the deviation of the TIMF energy from E_{Min} crosses the zero line. The slight buckling at the point Im(E)$\approx$ 2.5, visible in Fig.28, stems from adapting the TIMF iteration parameters to small imaginary parts of the energy and gives a hint about the numerical error inherent in the calculations. Extrapolation curves for other values of Re(E) and λ have been calculated but are not presented here. They show qualitatively the same behavior.

In short can say that the on–shell limit can be taken for TIMF as well as for SIRPA. We may conclude that SIRPA is an improvement over the mean field theory in this limit. Accordingly, SIRPA can be used for a microscopic, nonperturbative description of quantum mechanical scattering processes built upon a TIMF calculation. Besides the solution of the few dimensional SIRPA equations (an 8 dimensional matrix equation for two hole and particle orbitals as in our example), one needs two TIMF results for the amplitude D, where the second one is easy to get, because one has not to follow a whole path through the complex plane again. One may state, therefore, that the additional effort of including particle–hole correlations is reasonably small.

8 Summarizing the Results for the Solvable Model

The numerical results for the chosen model turn out to confirm the practicability of the SIRPA procedure. We list again its main points:

1. The SIRPA procedure is tractable with moderate efforts and yields an improvement over TIMF results.

2. While the TIMF approximation tends to yield a relatively smaller error for the larger of the two numbers, the real or imaginary part of amplitudes, SIRPA especially improves the other number, i.e the real part in the considered model.

3. The on–shell limit $\mathrm{Im}(E) \rightarrow 0$ is feasible for SIRPA.

4. The SIRPA procedure gives a hint for the occurrence of numerical problems of the TIMF calculations through sudden large jumps in the results.

5. The selection of SIRPA eigenvalues for the energy correction formula turns out to be easy. Furthermore, all the TDA eigenvalues had negative imaginary parts which therefore was a sufficient selection criterion for the SIRPA eigenvalues.

6. The SIRPA iteration always reached the given energy after two steps, and even one step yields a good approximation. This is numerically important, because every iteration requires one TIMF calculation.

7. It turned out to be sufficient to use only as many particle orbitals as there are hole orbitals in the SIRPA equations. Accordingly, the whole SIRPA procedure does not require much more numerical resources than a TIMF calculation even if working with more than two particles.

This shows that the basic idea of an inhomogeneous RPA is also numerically feasible.

9 Conclusion

A generalized random phase approximation has been introduced to include particle–hole correlations into the TIMF theory [1, 2] . For that purpose a second quantized version of TIMF based on three "natural" biorthogonal bases has been developed. The problem of finding matrix elements of an operator inverse can be reformulated as an eigenvalue problem with subsequent inversion of a complex function. Thus, the inhomogeneous problem of TIMF corresponds to a nonhermitian, homogeneous problem. For this homogeneous problem a nonhermitian generalization of the standard RPA can be found. The inhomogeneous RPA (IRPA) for the calculation of the matrix elements $D(E)$ consists of the inversion of the $E(D)$–relation obtained by a nonhermitian RPA. The issue of this paper has been to apply the inhomogeneous RPA to a solvable model and test the tractability of the new method and the quality of its results.

The numerical treatment leads to the necessity of working with square integrable particle orbitals in addition to the square integrable TIMF hole orbitals. This generalizes IRPA to SIRPA. To test SIRPA, a solvable model has been chosen. Because the nonhermitian RPA is equivalent to a canonical (but nonunitary) transformation, one is able to find the RPA energy correction without having first to calculate a complicated RPA state. The problem of dividing the eigenvalues into two appropriate groups, arising in a nonhermitian RPA when calculating the energy correction, turns out to be easy to solve in practice.

The SIRPA procedure is numerically practicable and leads to improved results compared to TIMF. Even the on–shell limit $\mathrm{Im}(E) \to 0$ can be taken. This means that SIRPA, built upon TIMF, can be used for a description of scattering processes. According to the experience with the above model, the numerical effort addded to that required by TIMF will be reasonably small.

Acknowledgements

The author is very grateful to B.G.Giraud and A.Weiguny for many fruitful and stimulating discussions.

References

[1] J. C. LEMM, submitted to Ann. Phys. (please insert reference) , and references therein

[2] J. C. LEMM, B. G. GIRAUD, AND A. WEIGUNY, *Phys.Rev.Lett.* **73** (1994), 420.

[3] B. G. GIRAUD, M. A. NAGARAJAN, AND C. J. NOBLE, *Phys. Rev. A***34** (1986), 1034.

[4] J. C. LEMM, doctoral dissertation, University of Münster, 1993.

[5] A. WIERLING, B. G. GIRAUD, F. MEKIDECHE, H. HORIUCHI, T. MARUYAMA, A. OHNISHI, J. C. LEMM, A. WEIGUNY, *Z.Phys. A***348** (1994), 153.

[6] B. G. GIRAUD, M. A. NAGARAJAN, AND A. WEIGUNY, *Phys. Rev. C***35** (1987), 55.

[7] B. G. GIRAUD, S. KESSAL, A. WEIGUNY, *J. Math. Phys.* **29** (1988), 2084.

[8] J. C. LEMM, A. WEIGUNY, AND B. G. GIRAUD, *Z. Phys. A***336** (1990), 179.

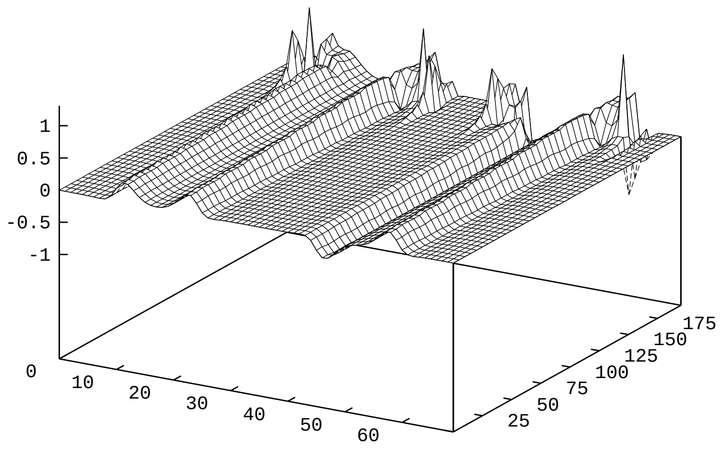

Figure 1: Real part of the even φ_1–orbitals (points 0 to 34) and odd φ_2–orbitals (points 35 to 70) on the one–dimensional grid during 200 iteration steps at Re(E)=6.25, Im(E)=0.1, $\lambda = 1.0$

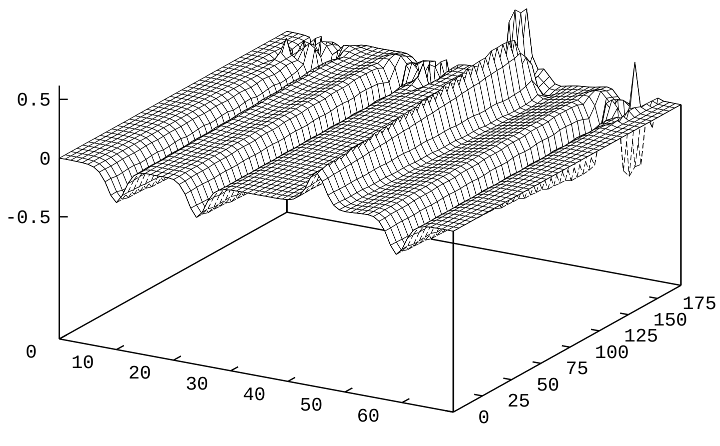

Figure 2: Imaginary part of the even φ_1–orbitals (points 0 to 34) and odd φ_2–orbitals (points 35 to 70) on the one–dimensional grid during 200 iteration steps at Re(E)=6.25, Im(E)=0.1, $\lambda = 1.0$

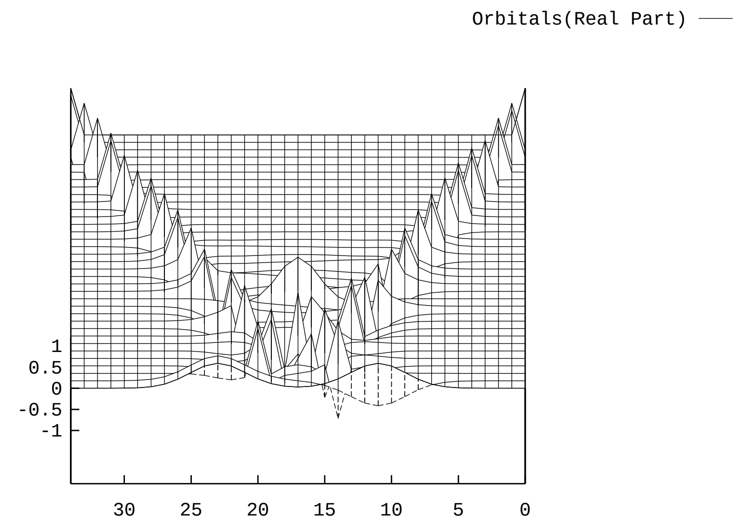

Figure 3: Real part of the IRPA-orbitals (holes and particles) for Re(E)=6.25, Im(E)=5.0 and $\lambda = 1.0$

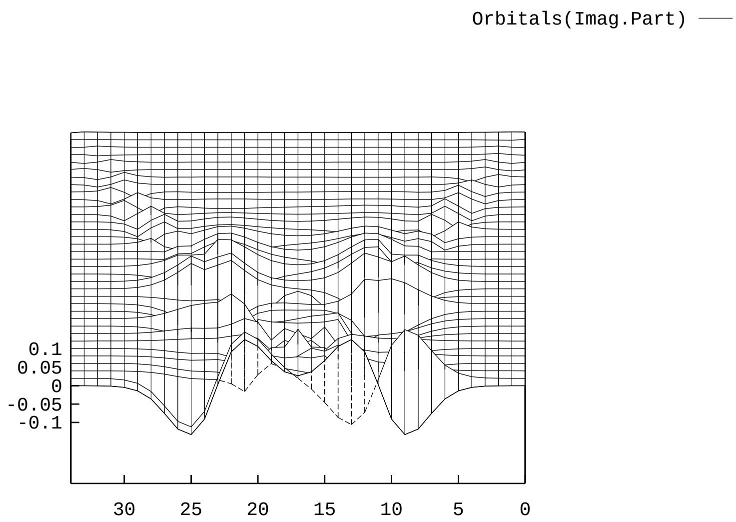

Figure 4: Imaginary part of the IRPA-orbitals (holes and particles) for Re(E)=6.25, Im(E)=5.0 and $\lambda = 1.0$

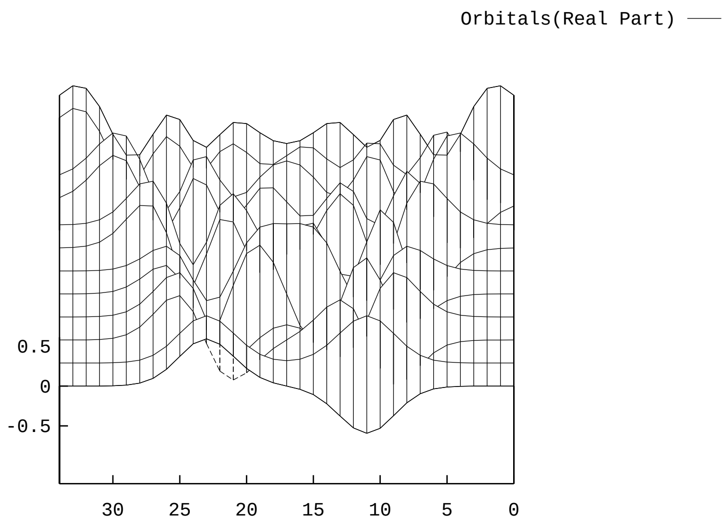

Figure 5: Real part of the square integrable SIRPA hole orbitals φ_1, φ_2 and 8 particle orbitals, for Re(E)=6.25, Im(E)=5.0 and $\lambda = 1.0$

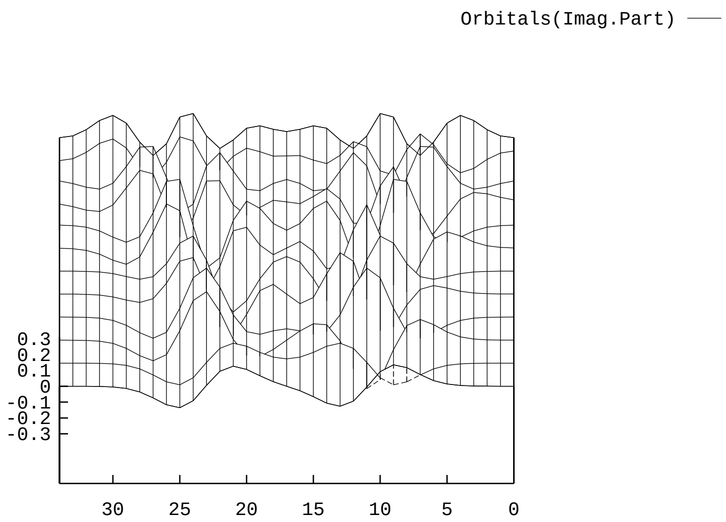

Figure 6: Imaginary part of the square integrable SIRPA hole orbitals φ_1, φ_2 and 8 particle orbitals, for Re(E)=6.25, Im(E)=5.0 and $\lambda = 1.0$

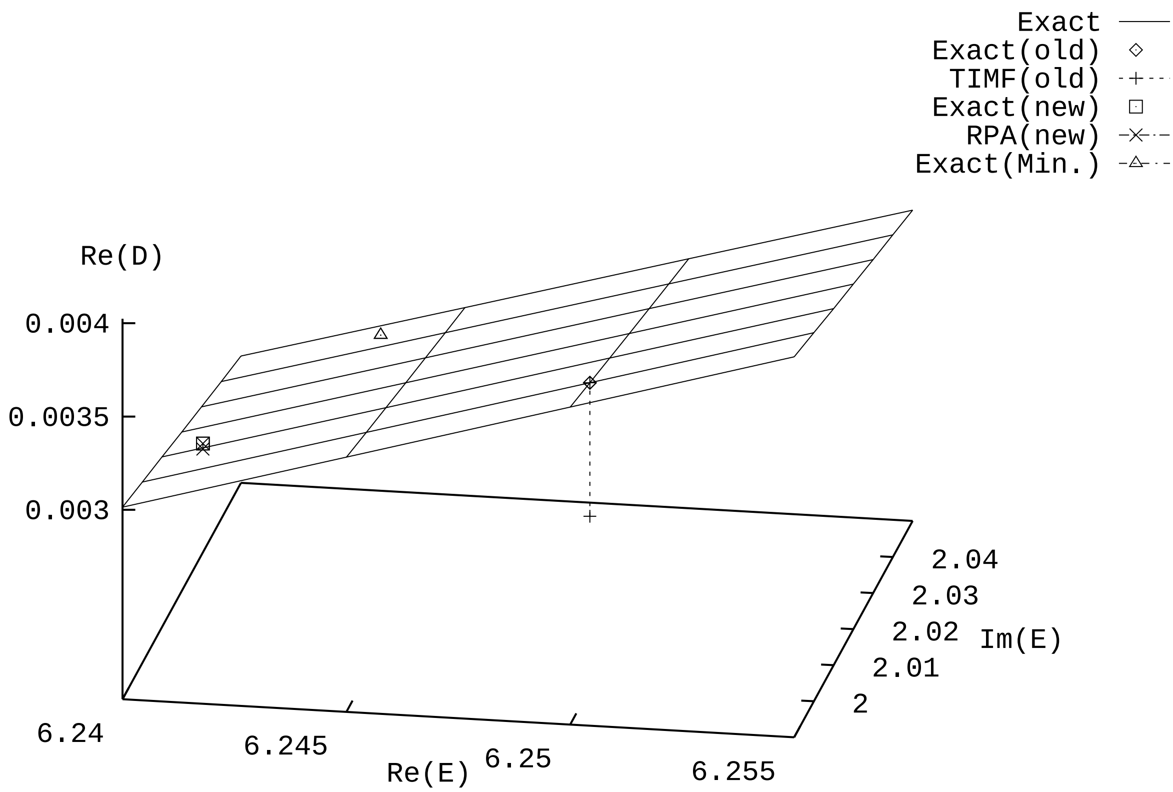

Figure 7: The SIRPA-procedure: Real parts of amplitudes D (exact and approximations) vs. Re(E) and Im(E), at constant boost $k = 2.5$ and $\lambda = 1.0$. The mesh shows the landscape of the real part of the exact amplitude $D_{Exact}(E)$ over the complex E–plane. Starting with a TIMF–approximation TIMF(old)=$D_{TIMF}(E_0)$ at energy $E_0 = 6.25 + i2.0$ for the exact amplitude Exact(old)=$D_{Exact}(E_0)$ the SIRPA–procedure gives a new energy $E_0' = E_0 + (\Delta E)_1$ so that RPA(new)=$D_{SIRPA}(E_0') = D_{TIMF}(E_0)$ is a much better approximation of Exact(new)=$D_{Exact}(E_0')$ at that new energy. The starting amplitude $D_{TIMF}(E_0)$ has the same numerical value as the exact amplitude Exact(Min.)= $D_{Min}(E_{Min})$ at energy E_{Min}, which therefore corresponds to the best possible corrected energy.

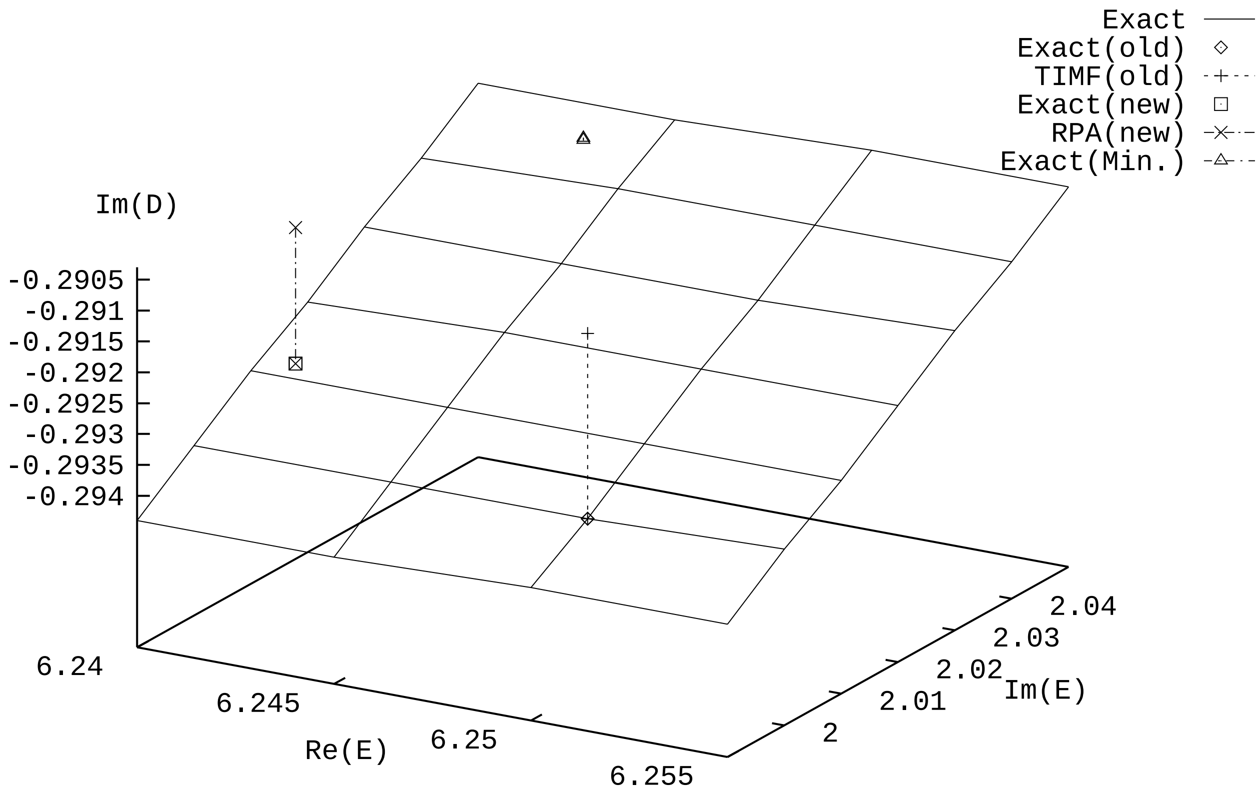

Figure 8: The SIRPA-procedure: Same as Fig.7, but for the imaginary parts of the various amplitudes D.

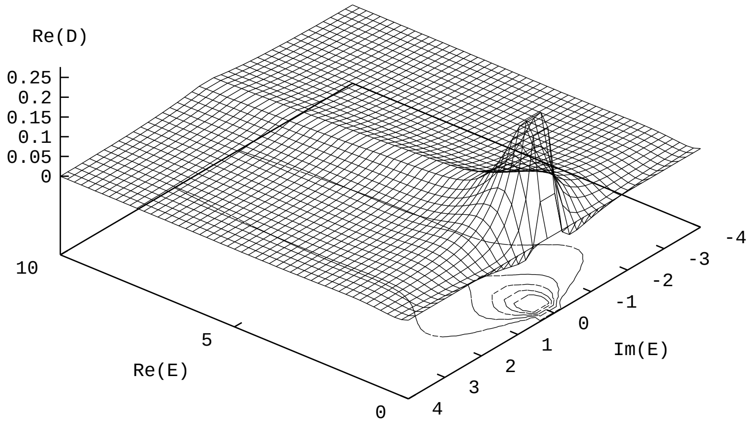

Figure 9: Real part of the exact amplitude $D_{Exact} = <\chi\,|\,(E-\mathcal{H})^{-1}\,|\,\chi>$ vs. $\mathrm{Re}(E)$ and $\mathrm{Im}(E)$, at $\lambda = 1.0$ and adapted boost $k = \sqrt{\mathrm{Re}(E)}$

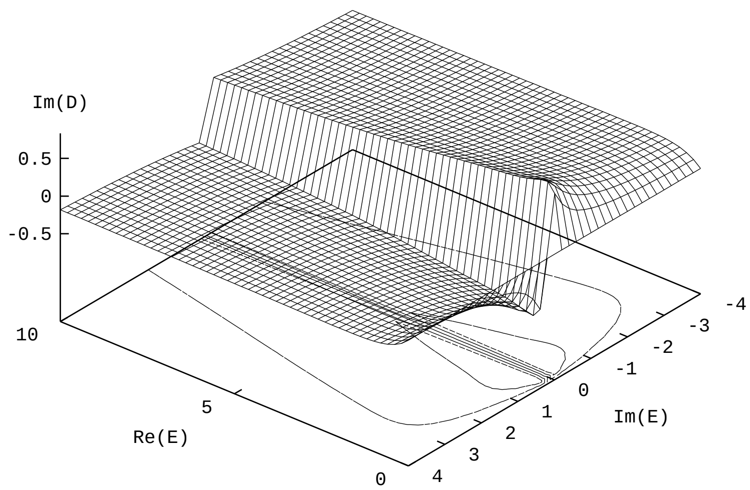

Figure 10: Imaginary part of the exact amplitude $D_{Exact} = <\chi\,|\,(E-\mathcal{H})^{-1}\,|\,\chi>$ vs. $\mathrm{Re}(E)$ and $\mathrm{Im}(E)$, at $\lambda = 1.0$ and adapted boost $k = \sqrt{\mathrm{Re}(E)}$

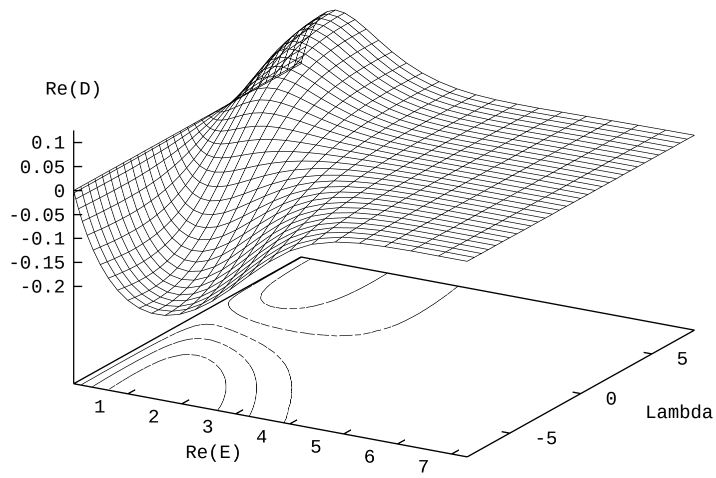

Figure 11: Real part of the exact amplitude $D_{Exact} = <\chi\,|\,(E-\mathcal{H})^{-1}\,|\,\chi>$ vs. Re(E) and λ , at Im(E) =2.0 and adapted boost $k = \sqrt{\mathrm{Re}(E)}$

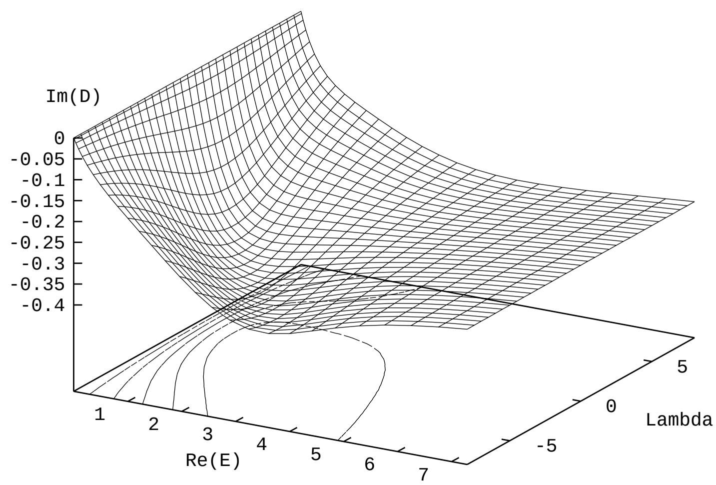

Figure 12: Imaginary part of the exact amplitude $D_{Exact} = <\chi\,|\,(E-\mathcal{H})^{-1}\,|\,\chi>$ vs. Re(E) and λ , at Im(E) =2.0 and adapted boost $k = \sqrt{\mathrm{Re}(E)}$

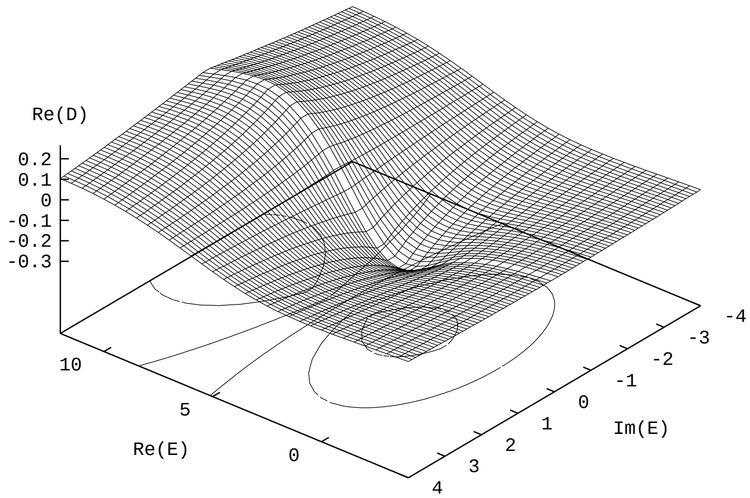

Figure 13: Real part of the exact amplitude $D_{Exact} = <\chi\,|\,(E-\mathcal{H})^{-1}\,|\,\chi>$ vs. Re(E) and Im(E), at $\lambda = 1.0$ and constant boost $k = 2.5(=\sqrt{6.25})$

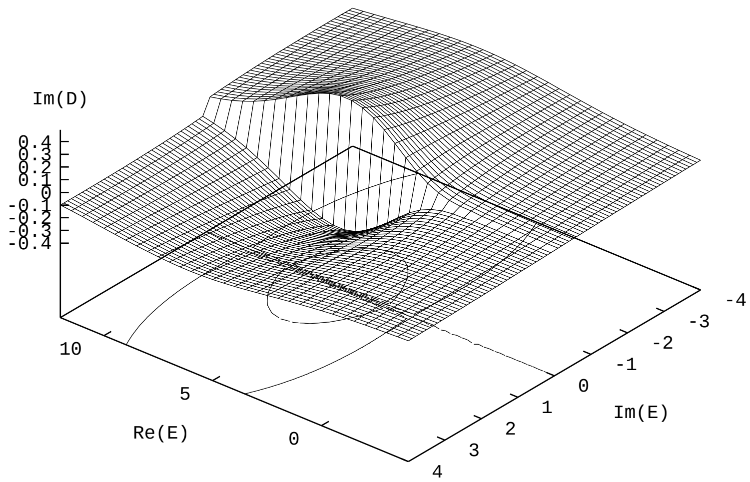

Figure 14: Imaginary part of the exact amplitude $D_{Exact} = <\chi\,|\,(E-\mathcal{H})^{-1}\,|\,\chi>$ vs. Re(E) and Im(E), at $\lambda = 1.0$ and constant boost $k = 2.5(=\sqrt{6.25})$

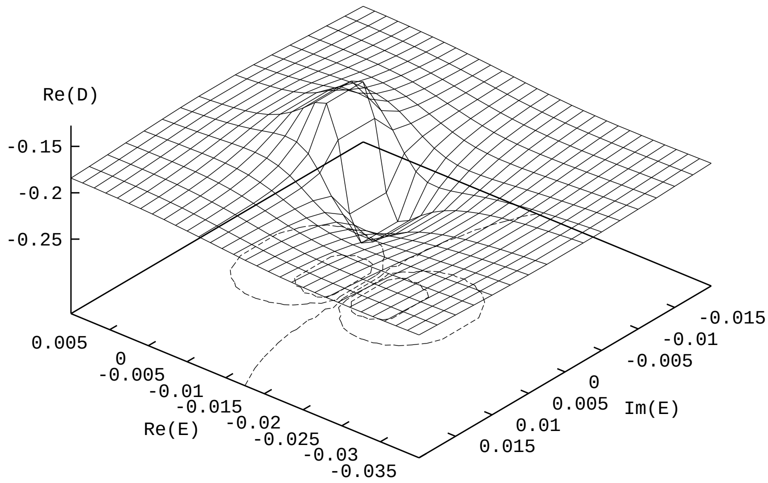

Figure 15: Real part of the exact amplitude $D_{Exact} = <\chi\,|\,(E-\mathcal{H})^{-1}\,|\,\chi>$ vs. Re(E) and Im(E), at $\lambda = 1.0$ and constant boost $k = 2.5$, reflecting the bound state of $\mathcal{H}$

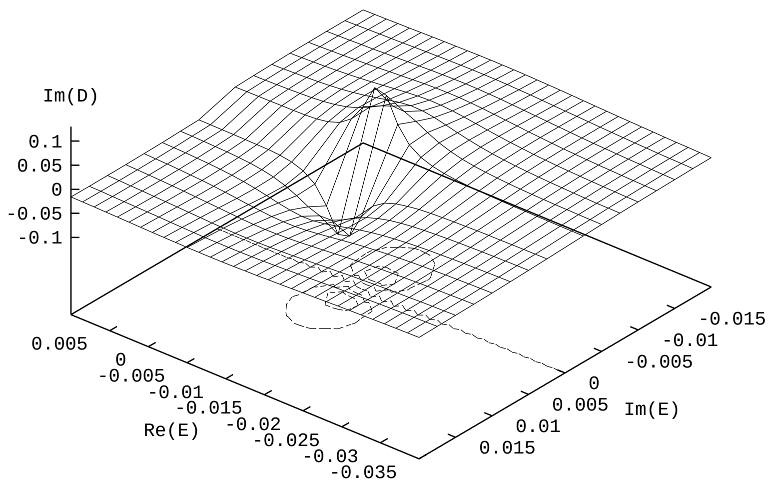

Figure 16: Imaginary part of the exact amplitude $D_{Exact} = <\chi\,|\,(E-\mathcal{H})^{-1}\,|\,\chi>$ vs. Re(E) and Im(E), at $\lambda = 1.0$ and constant boost $k = 2.5$, reflecting the bound state of $\mathcal{H}$

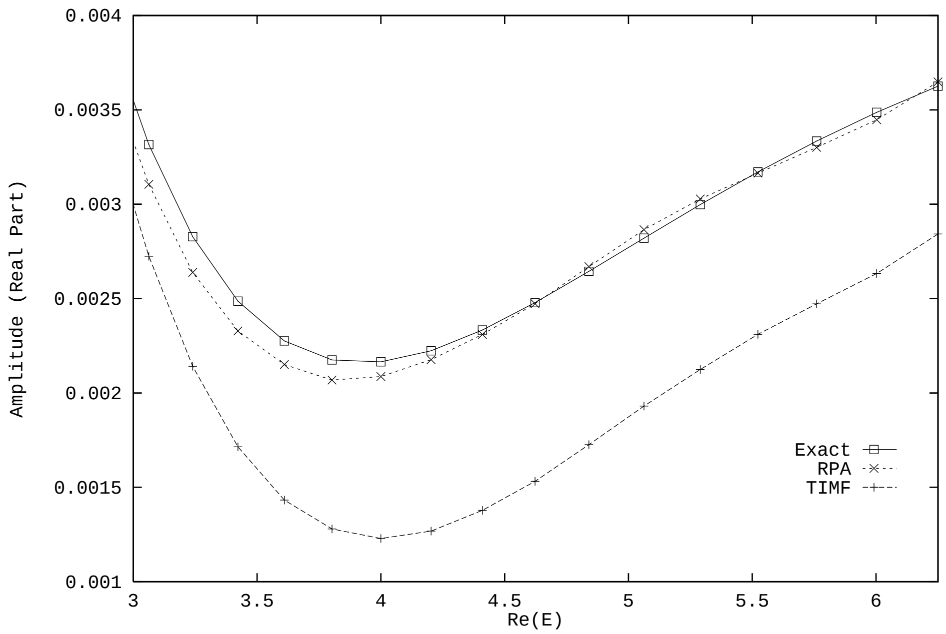

Figure 17: Real part of the exact, TIMF- and SIRPA-amplitudes vs. Re(E), at Im(E)=2.0 and $\lambda = 1.0$

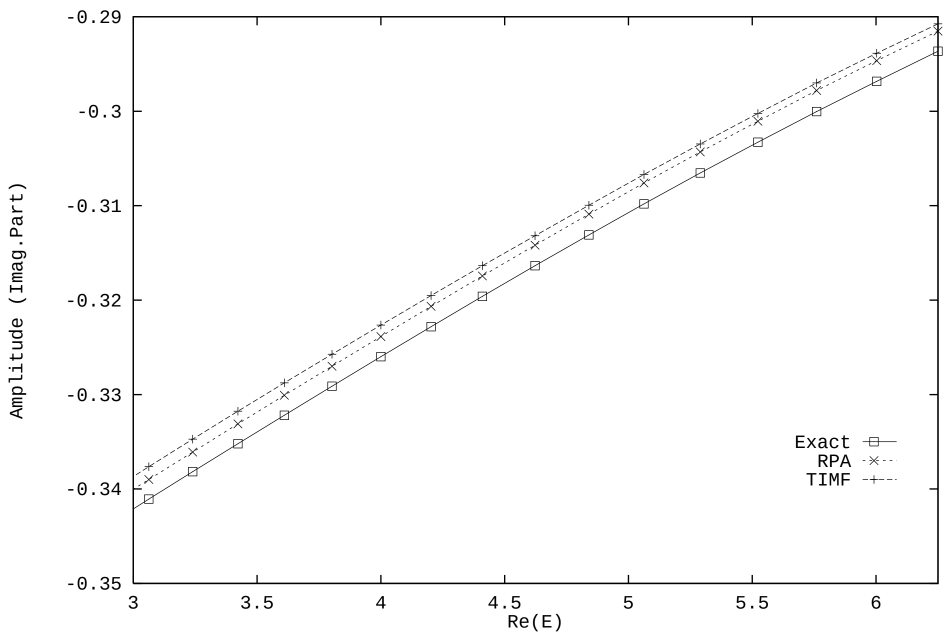

Figure 18: Imaginary part of the exact, TIMF- and SIRPA-amplitudes vs. Re(E), at Im(E)=2.0 and $\lambda = 1.0$

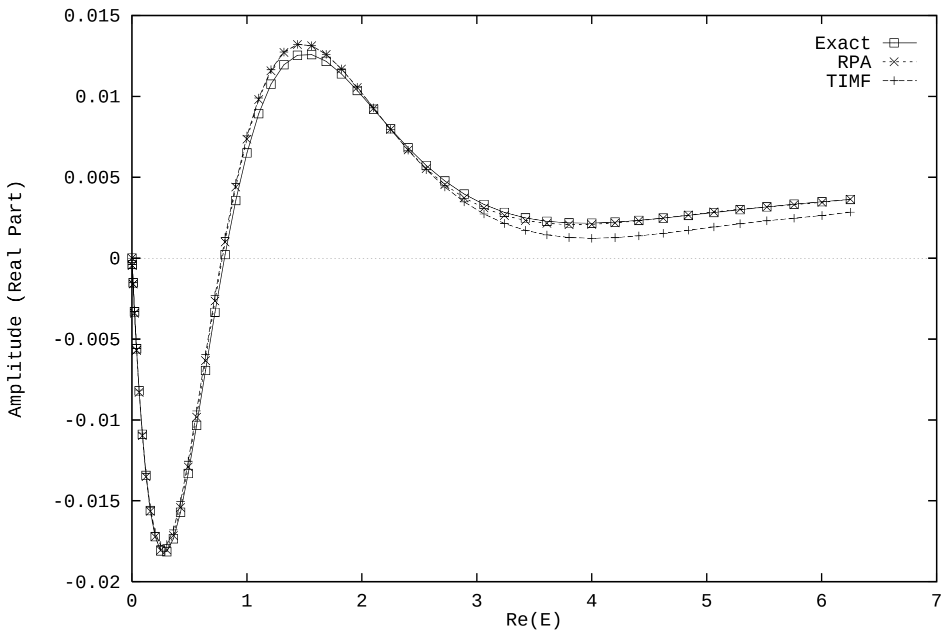

Figure 19: Real part of the exact, TIMF- and SIRPA-amplitudes vs. Re(E), at Im(E)=2.0 and $\lambda = 1.0$

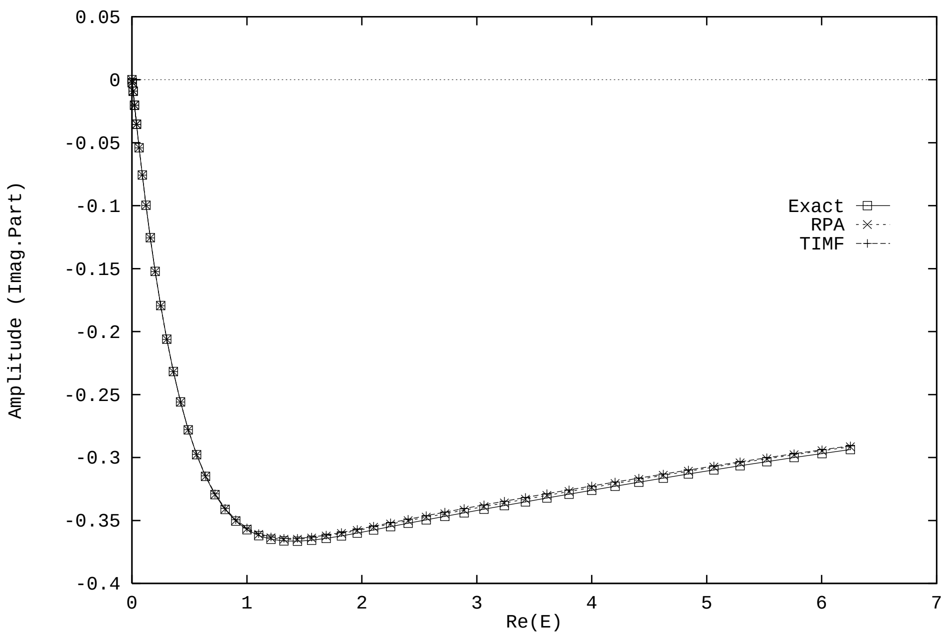

Figure 20: Imaginary part of the exact, TIMF- and SIRPA-amplitudes vs. Re(E), at Im(E)=2.0 and $\lambda = 1.0$

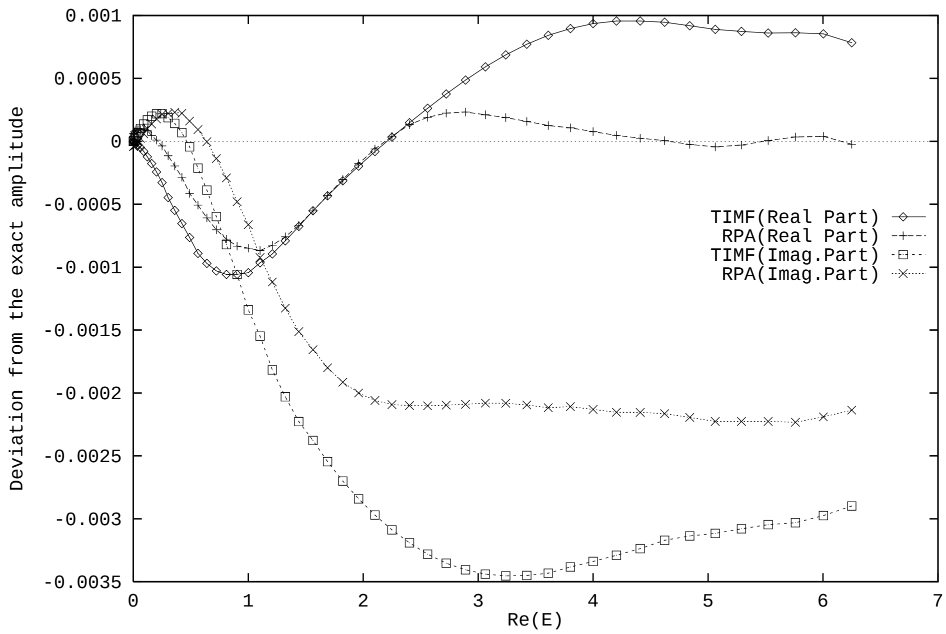

Figure 21: Deviation of the TIMF- and SIRPA-amplitudes from D_{Exact} vs. Re(E), at Im(E)=2.0 and $\lambda = 1.0$

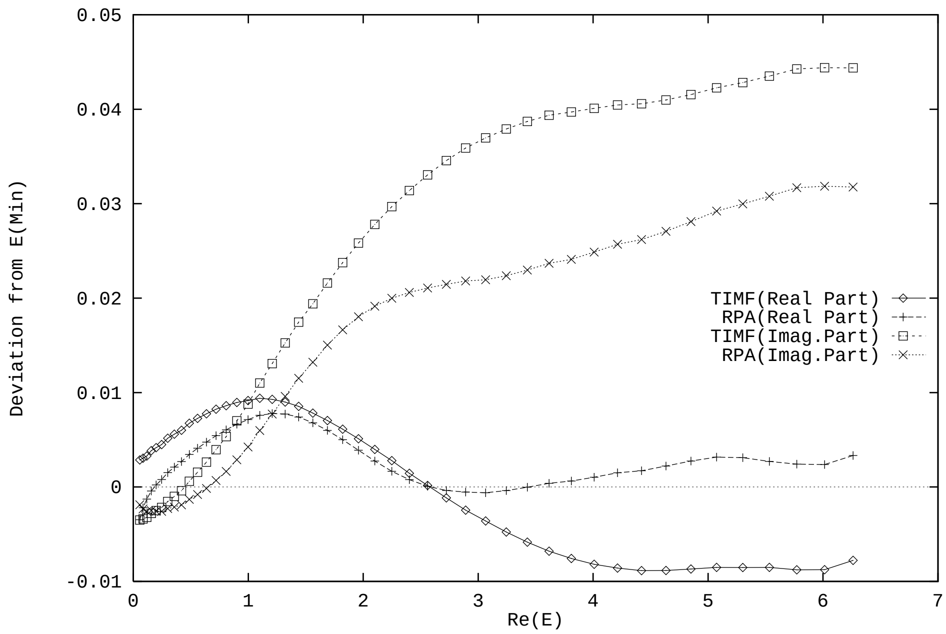

Figure 22: Deviation of the TIMF- and SIRPA-energies from E_{Min} vs. Re(E), at Im(E)=2.0 and $\lambda = 1.0$

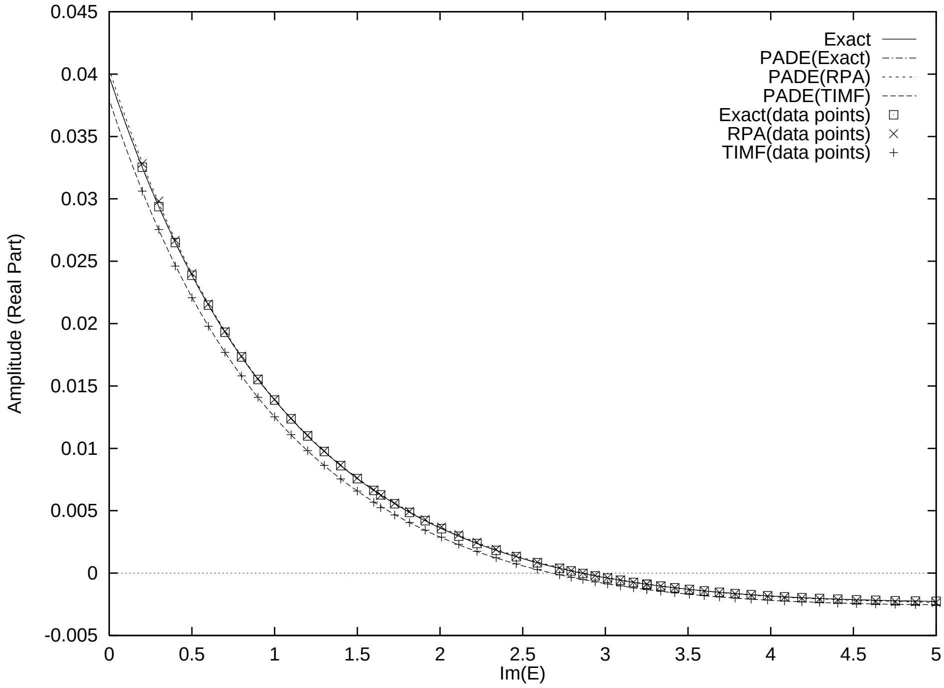

Figure 23: Rational fit functions for Re(D) with $n = 7$, at Re(E)=6.25 and $\lambda = 1.0$

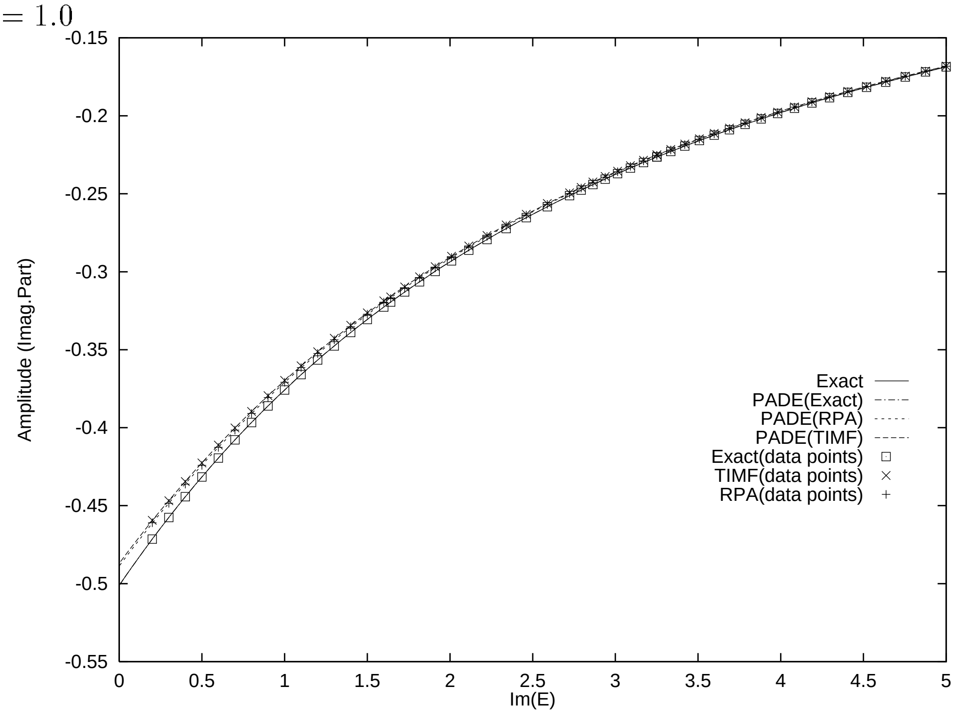

Figure 24: Rational fit functions for Im(D) with $n = 7$, at Re(E)=6.25 and $\lambda = 1.0$

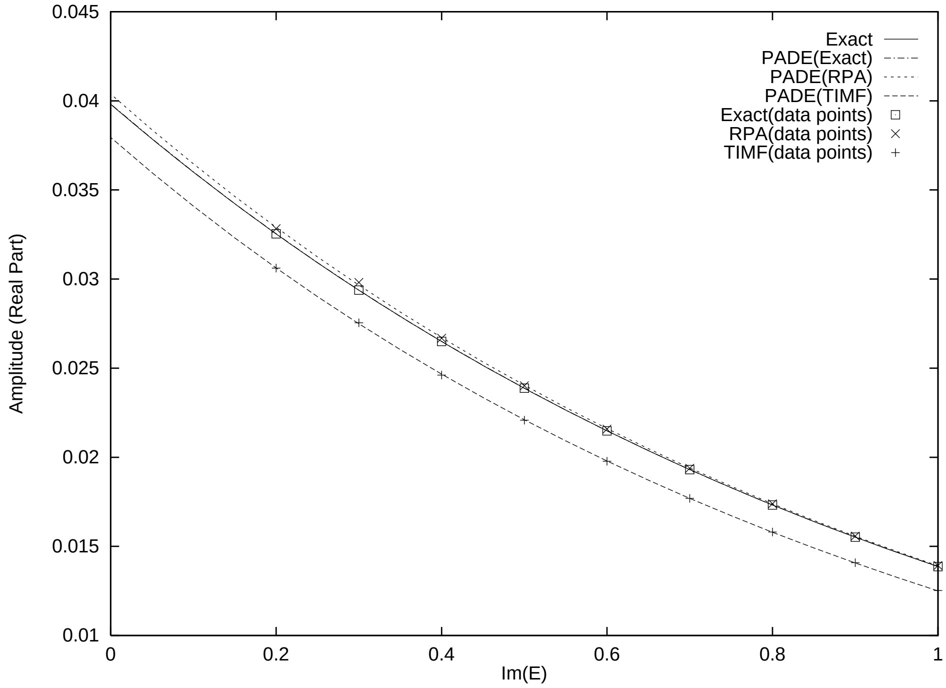

Figure 25: Rational fit functions for Re(D) with $n = 7$, at Re(E)=6.25 and $\lambda = 1.0$ (Same as Fig.23 with clipped range for Im(E))

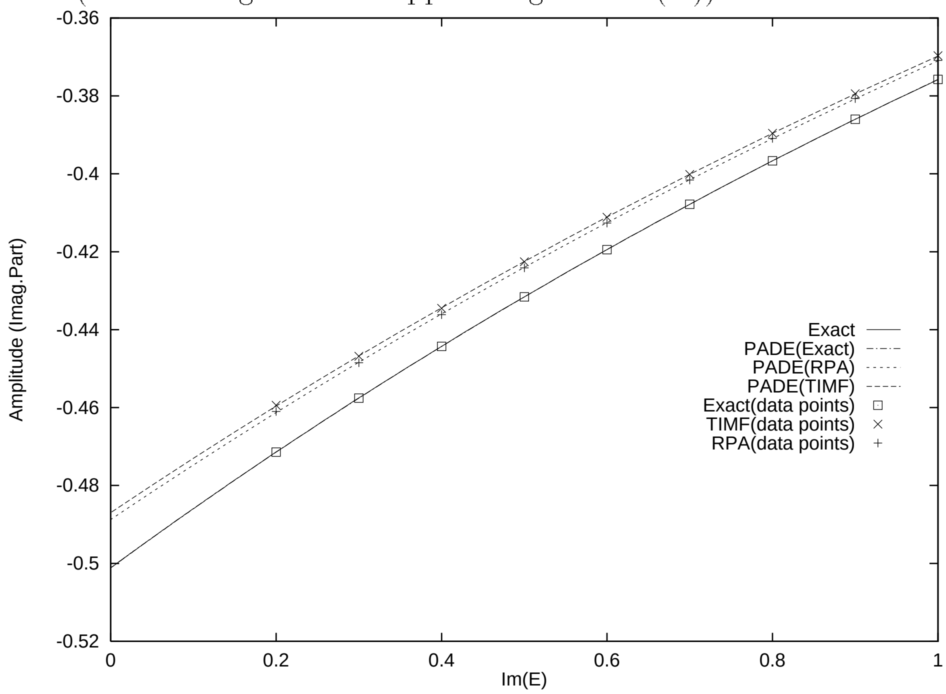

Figure 26: Rational fit functions for Im(D) with $n = 7$, at Re(E)=6.25 and $\lambda = 1.0$ (Same as Fig.24 with clipped range for Im(E))

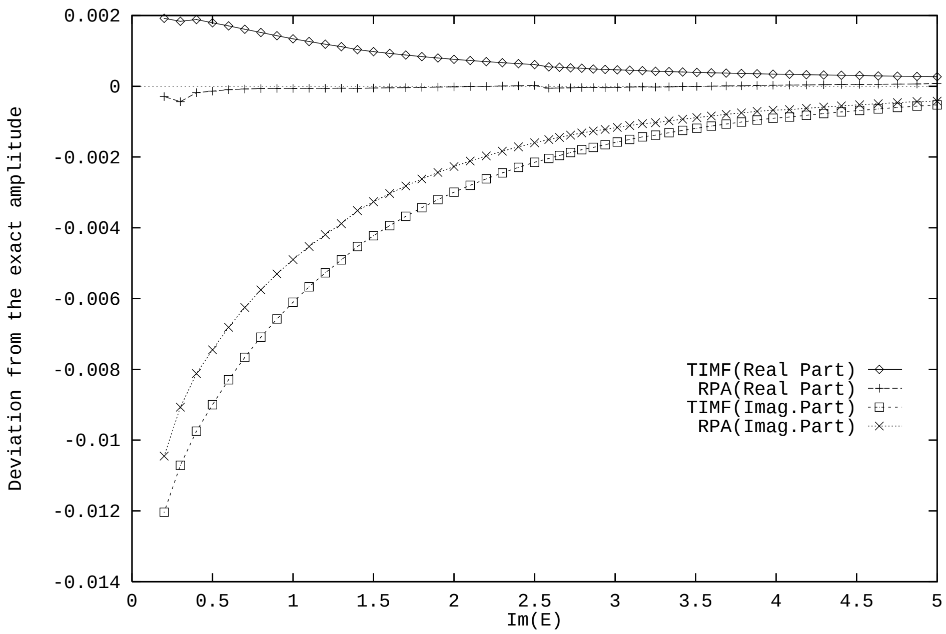

Figure 27: Deviation of TIMF- and SIRPA-amplitudes from D_{Exact} vs. Im(E), at Re(E)=6.25 and $\lambda = 1.0$

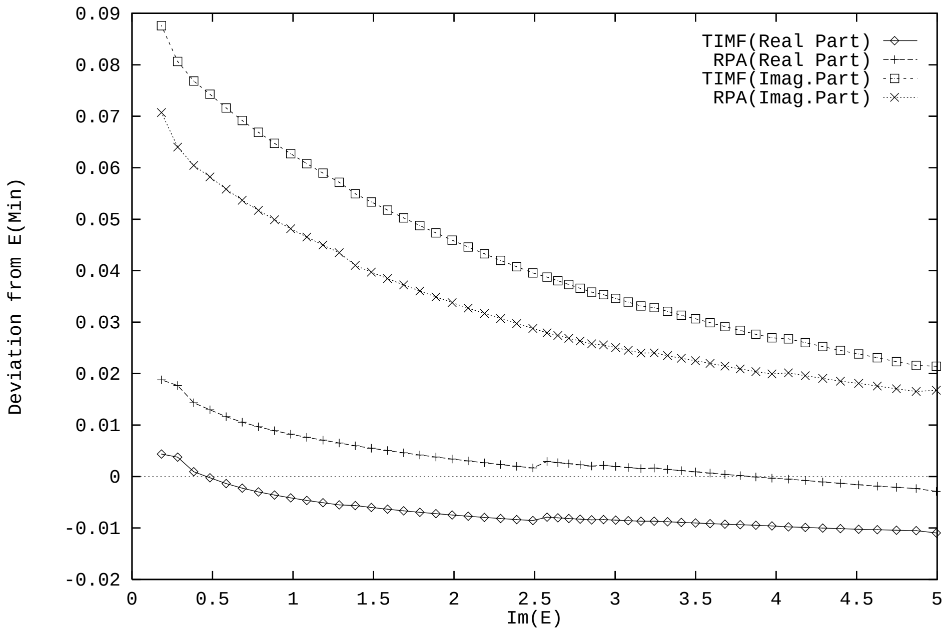

Figure 28: Deviation of TIMF- and SIRPA-energies from E_{Min} vs. Im(E), at Re(E)=6.25 and $\lambda = 1.0$